ELSEVIER

Surface Science 467 (2000) 58–84

surface science

www.elsevier.nl/locate/susc

Step-bunching transitions on vicinal surfaces with attractive step interactions

V.B. Shenoy [a,*], Shiwei Zhang [b], W.F. Saam [c]

[a] *Division of Engineering, Brown University, Providence, RI 02912, USA*
[b] *Department of Physics and Department of Applied Science, College of William and Mary, Williamsburg, VA 23187, USA*
[c] *Physics Department, The Ohio State University, Columbus, OH 43210, USA*

Received 8 February 2000; accepted for publication 24 May 2000

Abstract

We study vicinal crystal surfaces within the terrace–step–kink model on a discrete lattice. Including both a short-ranged attractive interaction and a long-ranged repulsive interaction arising from elastic forces, we discover a series of phases in which steps coalesce into bunches of n_b steps each. The value of n_b varies with temperature and the ratio of short- to long-range interaction strengths. For bunches with large number of steps, we show that, at $T=0$, our bunch phases correspond to the well-known periodic groove structure first predicted by Marchenko. An extension to $T>0$ is developed. We propose that the bunch phases have been observed in very recent experiments on Si surfaces, and we advance a conjecture explaining the exponent $\beta \approx 0.5$ describing the shape of the observed phase transition curves. Further experiments are suggested. Within the context of a mapping of the model to a system of bosons on a 1D lattice, the bunch phases appear as quantum n-mers. © 2000 Elsevier Science B.V. All rights reserved.

Keywords: Faceting; Green's function methods; Many body and quasi-particle theories; Monte Carlo simulations; Silicon; Step formation and bunching; Stepped single crystal surfaces

1. Introduction

The study of the equilibrium properties of a stepped vicinal crystal surface is important from technological and fundamental perspectives. The understanding of the surface morphology is key to phenomena such as epitaxial growth, chemical etching and catalysis. In addition, it also provides a fascinating example of a problem which has a much broader context, reaching, via a mapping onto a one-dimensional quantum chain, into the realm of 1D quantum liquids. In this paper we consider the morphology of vicinal surfaces in the case where step–step interactions are repulsive at large separations and attractive at short distances. Our work is aimed at elucidating the features of the surface morphology of miscut Si (113) surfaces observed in two sets of experiments. The first is that of the description of apparent tricritical phenomena observed in beautiful experiments by Song et al. [1–3] and Yoon et al. [4] on silicon surfaces miscut from the (113) direction in several very different directions. The second is the recent observations of multiple-height steps by Sudoh et al.[5,6] on vicinal (113) surfaces misoriented towards a low symmetry azimuth which is directed 33° away from the $[\bar{1}10]$ direction towards the $[\bar{3}\bar{3}2]$ direction.

Recent theoretical work [7,8] attempted to

* Corresponding author. Fax: +401 8639009.
E-mail address: shenoyv@engin.brown.edu (V.B. Shenoy)

0039-6028/00/$ - see front matter © 2000 Elsevier Science B.V. All rights reserved.
PII: S0039-6028(00)00664-6

explain the experiments of Song et al. in terms of a continuum model of steps interacting via a long-ranged repulsive elastic interaction and a short-ranged attractive interaction. This model produces a tricritical point, but it requires somewhat artificial tuning to give the observed coexistence curve exponent and fails to describe the observed bunching of steps on the vicinal surfaces coexisting with the (113) facet. The work reported in Ref. [8] has been in extended in Ref. [9] to suggest additional phases relevant to the observations of Yoon et al. [4]. Here we explore the consequences of retaining the discrete, atomic nature of steps on a crystal surface within the same model. We discover that the steps do not phase separate but instead can coalesce into bunches whose size depends on the relative strengths of the short- and long-range interactions and temperature. Vicinal surface phases can be characterized by widely separated n-bunches and transitions occur between phases having different values of n. We propose that the $n=2$, 3, 4 bunch phases produce the multiple-height steps seen by Sudoh et al. and that bunch phases with large n correspond to the two-phase coexistence regions of Song et al. and Yoon et al. [4].

For bunches with large numbers of steps, we show that, at $T=0$, our bunch phases correspond to the well-known periodic groove structure predicted by Marchenko [10]. While Marchenko's calculations are valid only at $T=0$, our theory predicts the evolution of the periodic groove structure as the temperature of the surface is raised. In addition, we show that Marchenko's phenomenological parameters like the edge energy can be determined in terms of the parameters that characterize the long- and short-range step–step interaction strengths. Because the phase transitions observed by Song et al. and Yoon et al. [4] occur in the limit of very large bunches with vanishing interbunch spacing, we are unable to describe details of the transitions. We do, however, provide a conjecture leading to a natural and robust explanation of the shape of the phase transition curves seen in the experiments. The relevance of the bunching transitions described here goes well beyond the crystal surface problem. In particular, the model provides opportunities to study many-body phenomena arising from coupling of modes on different length and energy scales.

In the following section, we introduce our model, the terrace–step–kink model (TSK) [11], and develop the mapping to the hard-core boson problem. In Section 3, we analyze the model in what we call the extreme dilute limit (EDL), where bunches are widely separated. For $T=0$, the exact solution clearly reveals the essence of our problem, a series of first-order bunching transitions. For bunches with large numbers of steps, we show the connection between the bunches phases and the periodic groove structure predicted by Marchenko [10]; this demonstration extends beyond the EDL, to the case of large bunches, not necessarily widely separated. In the EDL, using exact diagonalization on small systems to reveal the nature of the bunching transitions, we develop the physics for $T>0$. Section 4 uses phenomenology coupled with scaling arguments to include interactions between bunches in the case that they are widely separated, and to study the effects of the interactions on transitions from one bunch size to another. In Section 5 we use quantum Monte Carlo simulations to check the results of exact diagonalization by explicitly looking at particle–particle correlations through a series of bunching transitions. Section 6 gives a detailed comparison of our results with continuum theories. In Section 7 we compare the key experimental findings with the predictions of the theory. Differences and similarities are highlighted, and directions for further development of the theory are suggested. We conclude by discussing the main results and pointing directions of future research. A brief description of this work has already been reported [12].

2. Hamiltonian of interacting steps

In order to study the thermodynamics of surfaces that are miscut by a small amount from a reference surface, we will first derive the surface free energy by treating the miscut angle and temperature as thermodynamic variables. The surface free energy will be expressed in terms of the ground state energy of a one-dimensional quantum mechanical model that is derived using transfer

matrix methods. The model we use is the TSK model. This lattice model can be mapped onto an equivalent quantum mechanical model of interacting spin-less fermions or hard-core bosons. Details are found in earlier work [11,13][1,2] .

In the study of interacting steps it is common to use both discrete and continuum models. It is important to understand the limiting process which brings out the equivalence of the two models. While it is generally true that, when the limiting process is carried out properly, it is possible to switch between the models, caution should be exercised to make conclusions about one model based on the results of the other. The bunching transition is one such example, where the cut off distance (lattice spacing) in the lattice model plays a crucial role. As we discuss in Section 7, there is nothing corresponding to bunching transitions in the continuum model; they are purely lattice effects. On the other hand, to study the interactions between steps whose average separation is much larger than the lattice spacing, one can use either the lattice model or the continuum model.

We will now turn our attention to the TSK model and (1) derive the quantum Hamiltonian in terms of hard-core boson operators, (2) make the connection between the free energy of the surface to the ground state energy of the quantum mechanical system and (3) derive the connection between the kink energy in the lattice model and step stiffness in the continuum model.

2.1. Terrace–step–kink model

Let us consider a square lattice with M rows and L columns as shown in Fig. 1, where steps between terraces are specified by bonds on this lattice. Let the steps in the TSK model run parallel to the y-axis, so that the slope of the crystal face is in the x-direction. One can specify a configuration of this system by specifying the x-coordinates of each of the N steps at each of the y-coordinates. The lattice spacing in the x and y direction is denoted by a_x and a_y respectively. The density of steps is related to the slope of the interface under consideration through the relation $s=\tan\theta=(Na_z/La_x)$, where a_z is the lattice parameter in the z-direction or the step height. For notational convenience we specify a configuration by the state vector $|x_1, x_2, \ldots, x_N\rangle_k$, where x_j denotes the position of the jth step in the kth row. The position of the step can only change by ± 1 between the rows by creating a kink. The transfer matrix describes the propagation of steps from row to row. It can be determined by a kink energy Γ, an energy η_0 for a unit length of the straight step, and an interaction energy V_{ij} between parallel straight pieces of steps labeled i and j. To render interactions between different rows (steps interacting at different values of y) tractable, we treat them in an average way: we compute V_{ij} as the interaction between a unit length of step at i and an infinite straight step at j. We expect this approximation to preserve the qualitative physics of interest here. In going from row k to row $k+1$, if the ordinates of p steps are unchanged while the other $(N-p)$ steps change by ± 1, then the transfer matrix element has a contribution $\exp(-\beta a_y N\eta_0-\beta\Gamma(N-p))$, where $\beta=1/k_{\mathrm{B}}T$. The matrix element vanishes if $x_i=x_j$ for $i\neq j$, i.e. the steps do not cross. The transfer matrix element also has a multiplicative element contribution from the step interactions, that can be written as

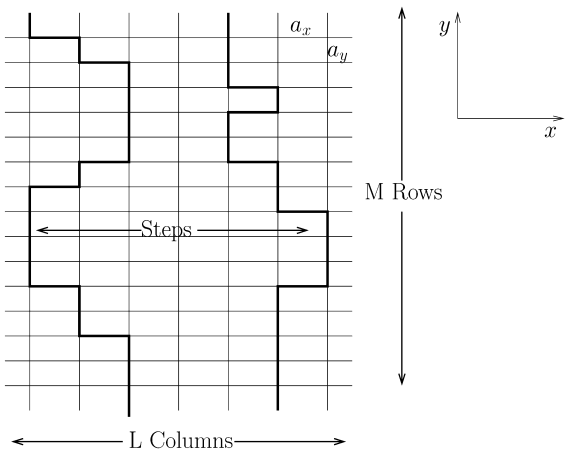


Fig. 1. Geometry for the TSK model. The steps between terraces are indicated by bonds on the lattice.They run parallel to the y-axis on an average.

[1] For a general review of fermionic methods, see Ref. [14].

[2] Numerical evaluation of the free energy of a vicinal surface using fermionic methods can be found in Ref. [15].

$\exp(-\beta a_y \sum_{i<j} V_{ij})$. A convenient operator representation is obtained by associating a step creation operator $a_j^\dagger$ for a step at x_j in row k: $a_j^\dagger a_j$ denotes a straight step while $a_{j+1}^\dagger a_j$ and $a_j^\dagger a_{j+1}$ denote a kink to the right and to the left, respectively. The as are defined so that $(a_j^\dagger)^2 = 0$, which imposes the non-crossing condition. This gives us a choice of a fermionic or hard-core bosonic representation of as. We adopt the hard-bosonic representation, where as satisfy the usual bosonic commutation relations

$$[a_i, a_j] = [a_i^\dagger, a_j^\dagger] = [a_i, a_j^\dagger] = 0, \tag{1}$$

when $i \neq j$ and satisfy anti-commutation relations on the same site, i.e.

$$[a_i, a_i]_- = [a_i^\dagger, a_i^\dagger]_- = 0, \quad [a_i, a_i^\dagger]_- = 1. \tag{2}$$

The on-site anti-commutation relations take care of the hard-core condition $(a_j^\dagger)^2 = 0$. This representation is equivalent to the fermion representation introduced in Ref. [11]. The fermion operators that anti-commute on different sites are related to the hard-core boson operators through the unitary Jordan–Wigner transformation [16].

Let us denote the $(N \times N)$ transfer matrix by $\hat{\mathscr{T}}$. For mathematical convenience we take the continuum limit in the y-direction (i.e. we take the limit of the lattice spacing $a_y \to 0$). In this limit to first order in a_y, the transfer matrix can be written as

$$\hat{\mathscr{T}} = \hat{1} - \frac{a_y}{k_B T}\mathscr{H}, \tag{3}$$

where $\hat{1}$ is the identity operator and the quantum Hamiltonian, $\mathscr{H}$, is defined as

$$\mathscr{H} \equiv \eta(T)\sum_i n_i - t\sum_i [a_{i+1}^\dagger a_i + a_{i+1} a_i^\dagger - 2n_i] + \sum_{(i,j)} V_{ij} n_i n_i. \tag{4}$$

Here (i, j) is used to denote a sum over distinct pairs of bosons, $n_i = a_i^\dagger a_i$, and the free energy of a straight step $\eta(T) = \eta_0 - 2t$, where the hopping parameter t is defined as

$$t = \lim_{a_y \to 0} \frac{\exp(-\beta\Gamma)}{\beta a_y}. \tag{5}$$

It should be noted that the kink energy is a function of a_y and diverges in the limit of vanishing a_y, but the ratio given by Eq. (5) remains finite. Note that since t is a monotonically increasing function of T which vanishes as $T \to 0$, t itself serves as an effective temperature variable.

The eigenvalues of the transfer matrix can be related to the projected surface energy of the miscut surface through the relation [11]

$$f(s) = \frac{\gamma(s)}{\cos\theta} = \gamma_0 - \frac{k_B T}{MLa_x a_y} \log(\mathrm{Tr}[\hat{\mathscr{T}}^M]), \tag{6}$$

where γ_0 is the surface tension of the reference surface and $\gamma(s)$ is the free energy per unit area of the miscut surface, i.e. the surface tension. In the continuum limit where Eq. (3) is satisfied, the projected free energy can be related to the ground state energy $E_0[N, T]$ of $\mathscr{H}$ through

$$f(s) = \gamma_0 + \frac{E_0[N, T]}{La_x}. \tag{7}$$

This relation can be used to relate the physical properties of the surface such as the curvature, stiffness etc. to the ground state energy of the hard-core boson system. We now turn to a discussion of the form of the step–step interactions that will enable us discuss the physics of faceting transitions.

2.2. Step–step interactions

In this paper we consider step–step interactions consisting of a repulsive long-range part and an attractive short-range part. We write the inverse square long-range part in the form

$$V_{i,j}^{\mathrm{lr}} = \frac{G}{|i-j|^2}, \tag{8}$$

and the short-range part as

$$V_{i,j}^{\mathrm{sr}} = -\sum_{k=1}^{n_s} U_k \delta_{|i-j|,k}, \tag{9}$$

where δ is the usual Kronecker delta. The quantity G has contributions arising from the elastic interactions as well as from the electronic charge rearrangements along the steps [11]. The elastic

part of G depends on the elastic constants of the crystal; for isotropic crystals it has the form [17,18][3]

$$G=2\,\frac{(1-\nu^2)\mathbf{f}^2}{\pi E a_x^2}, \tag{10}$$

where E and ν are the Young's modulus and Poisson's ratio respectively and $\mathbf{f}$ is the strength of the vector surface dipole force at a step. In this paper we will focus on crystals where the elastic contribution dominates the long-range part of step interactions, so that $G>0$ [4]. The short range potential depends on the details of the step–step interactions on atomic scales and has to be worked out from a microscopic calculation. There is ample experimental evidence [1–3,20–22] that this quantity can be attractive, i.e. $U_k>0$, on a few lattice spacings from the step[5]. The purpose of this paper is to explore the phases of vicinal surfaces in crystals with $G>0$ and $U_k>0$. In the remainder of the paper we will consider the case $n_s=1$ and $U_1\equiv U$, though in Section 7 we comment on the physics of systems with $n_s>1$. From this point on, we will focus on the Hamiltonian $\mathscr{H}$, written in the form

$$\mathscr{H}=\eta(T)\sum_i n_i - t\sum_i [a_{i+1}^\dagger a_i + a_{i+1}a_i^\dagger - 2n_i] + \sum_{(i,j)}\left[\frac{G}{|i-j|^2}-U\delta_{|i-j|,1}\right]n_i n_j. \tag{11}$$

2.3. Step stiffness and kink energy

In the study of the thermodynamics of steps it is very common to use a continuum model, where the Hamiltonian of a single step with coordinate $y(x)$ is written as

$$H=\frac{\Sigma}{2}\int\left(\frac{\mathrm{d}y}{\mathrm{d}x}\right)^2\mathrm{d}x, \tag{12}$$

where Σ is the step stiffness. For a single step it is instructive to make the connection between the kink energy in the lattice model and the stiffness in the continuum model. To this end, in Appendix B we derive, within the lattice model, the free energy of the step. By comparing the energies of the continuum model and the lattice model, we see that the step stiffness can be written as

$$\Sigma=\lim_{a_y\to 0}\frac{k_B T}{2a_x^2}\left(\frac{a_y}{\exp(-\beta\Gamma)}\right)=\frac{(k_B T)^2}{2a_x^2 t}. \tag{13}$$

The above equation is key in understanding the connection between the discrete and continuum models. We will return to this equation when we discuss the stiffness of step bunches.

3. Phase diagram in the extreme dilute limit

The form of the interaction that we have considered for the step interactions has competing components acting at different length scales. As noted before, we will focus on the case where there is an attractive potential on the near neighbor site only, i.e $n_s=1$ and $U_1\equiv U$. We now show that a number of features of this many-body system can be inferred from exact diagonalization of small systems in conjunction with some simple analytical calculations. In the discussions to follow, we will present simple physical arguments to show that for sufficiently attractive interactions, the steps on the surface rearrange themselves into bunches at low temperatures. At $T=0$, where the entropic effects are unimportant, the bunch size is completely determined by the ratio of the strengths of the attractive and repulsive interactions, i.e. U/G. With increasing temperature, the steps start peeling off from the bunches in a series of bunching transitions. In the extreme dilute limit (the details of which will be clear in the discussions to follow), we obtain a phase diagram that shows these bunching transitions as a function of temperature.

[3] The result for anisotropic crystals can be found in Appendix A.

[4] In addition to elastic interactions between steps, there can also be contributions to the inverse square potential from dipolar interactions arising from charge rearrangements on steps [11]. Unlike elastic interactions, these can have either sign. In metallic crystals oscillatory interactions mediated by conduction electrons [19] may play a role.

[5] A theoretical discussion of the origin of attractive step–step interactions is given in Ref. [19].

3.1. Phase diagram at $T=0$

Let us now consider the limit $t\to 0$, where the hopping part of the Hamiltonian Eq. (11) can be completely ignored. This corresponds to taking the zero temperature limit of the vicinal surface. In this limit, the energy of the system is obtained by minimizing the total potential energy, and depends on the single parameter U/G. A little reflection reveals that in the dilute limit, the minimum energy configuration for a given U/G consists of bosons in bunches of size n_b that are well separated from each other. In a bunch, the bosons sit next to one another. For a bunch of size n_b, the energy per boson is given by

$$\epsilon(n_b) \equiv \frac{E_0[N, T=0, n_b]}{N} = \eta(0) - U\left[\frac{n_b - 1}{n_b}\right] + G\left[\frac{1}{n_b}\sum_{i=1}^{n_b-1}\frac{n_b - i}{i^2}\right] + O((N/L)^2), \qquad (14)$$

where the term $O((N/L)^2)$ comes from bunch–bunch interactions and is small in the dilute limit. We call the limit in which the bunch interactions are completely ignored, the 'extreme dilute limit' (EDL). A straightforward minimization of $\epsilon(n_b)$ in the EDL reveals the phase diagram shown in Fig. 2a, where the circles marked on the U/G axis separate bunches that differ in size by one. With increasing U/G, the bunch size keeps increasing; for $U/G<1$ the bunch size is 1, for $1<U/G<1.5$ the bunch size is 2, for $1.5<U/G<1.83$ the bunch size is 3, for $1.83<U/G<2.08$ the bunch size is 4 and so on. At the circles marked in Fig. 2a (i.e. at $U/G=1$, 1.5, 1.83, 2.08, …) there is a coexistence of bunches that differ in size by one. From the graphs of the energy per boson versus U/G shown in Fig. 2b for different n_bs, we see that the slope at the points where these curves intersect are not the same. The $T=0$ bunching transitions brought about by changing U/G can then be considered first order.

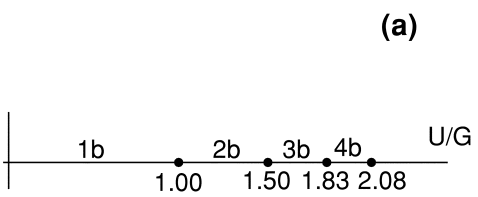
With increasing U/G, the spacing between the regions that differ in bunch size by one becomes smaller and smaller. For large U/G, Eq. (14) becomes

$$\epsilon(n_b) = \epsilon_\infty + \frac{\epsilon_e}{n_b} - \frac{G}{n_b}\ln n_b + O\left(\frac{1}{n_b^2}\right), \qquad (15)$$

where $\epsilon_\infty = \eta(0) + \pi^2 G/6 - U$ is the energy per step in a large bunch, $\epsilon_e = U - G - GC$ is the energy associated with the ends of the bunch, and $C=0.577$ is Euler's constant. Minimizing $\epsilon(n_b)$ in Eq. (15) with respect to n_b leads to a bunch size given by

$$n_b \approx 0.561\exp(U/G), \quad U/G \gg 1, \qquad (16)$$

which indicates that bunch size diverges rapidly with increasing U/G.



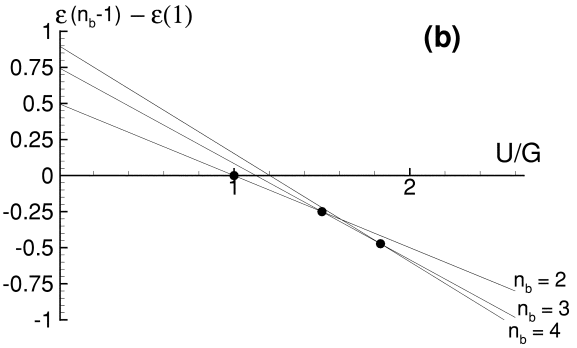


Fig. 2. (a) $T=0$ phase diagram of the vicinal surface plotted as a function of the ratio of the near neighbor attractive interaction U and repulsive inverse square interaction G. The dots separate regions with stable bunch sizes that differ by one (the bunch sizes are indicated in the figure as 1b, 2b etc.). (b) Plot of the difference in energy per boson in an n_b bunch and the energy of a 1-bunch. At the points indicated by dots, the bunch size corresponding to the minimum of the energy difference increases by one. The slope of the line in (b) for a bunch with n_b bosons is $(n_b-1)/n_b$.

The above calculation has shown that the steps split themselves into bunches in the EDL at $T=0$. In the next subsection, we study the unbinding of the steps with increasing temperature in the EDL. First, however, we connect the result Eq. (16) for large bunches with the earlier work of Marchenko [10].

For the case at hand, if elastic interactions are ignored, steps have only the short-ranged attractive interaction $-U$. Here there is a coexistence (see, e.g. Ref. [11]) between the flat, step-free facet and the facet formed when there are steps at each site. The latter facet is inclined at an angle $\theta_0=\tan^{-1}(a_z/a_x)$ with respect to the former. All facets with angles θ such that $0<\theta<\theta_0$ are unstable and will decompose into coexisting facets with angles 0 and θ_0. Marchenko [10][6] showed that when elastic interactions are taken into account, facets with $0<\theta<\theta_0$ become stable, being formed from an array of grooves as shown in Fig. 3. Each groove is composed of a step-free portion followed by a step bunch, in the terminology of this paper. In fact this 'groove' phase looks just like a bunch phase with n_b large. It should then be possible to connect Marchenko's results with those of Eq. (15) in the limit, the EDL, where the bunches are widely separated. This corresponds to the case of small θ and small θ/θ_0. Marchenko also assumes small θ_0, as will we in making the connection to his work. In terms of the geometry shown in Fig. 3, we have

$$n_b=\frac{L_g\sin\theta}{a_z}\approx\frac{L_g\theta}{a_z}, \tag{17}$$

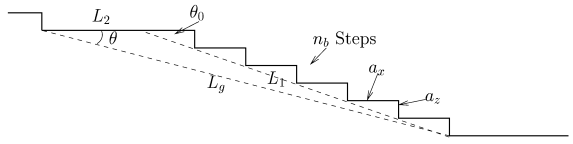


Fig. 3. Periodic groove structure proposed by Marchenko. The figure shows the repeating groove structure (length L_g), the flat facet (length L_1) and the stepped facet (length L_2). The case $n_b=6$ is shown here for graphical simplicity. Marchenko's calculation applies only for n_b large.

[6] Note that a factor of 2 should multiply the second line in the equation at the bottom of the first page of this article.

where L_g is the length of a Marchenko groove and $a=\sqrt{a_x^2+a_z^2}$. The surface energy per unit area of the grooved surface is

$$\begin{aligned}\gamma_g(\theta)&=\frac{\gamma_0L_2+\gamma(\theta_0)L_1}{L_g}\\&=\frac{\gamma_0\{L_2+L_1\cos\theta_0[1+\epsilon_\infty/\gamma_0a_x]\}}{L_g}\\&\quad-\frac{G}{L_g}\ln\left(L_g\theta_0a^*\theta_0\right)\\&\equiv\gamma_0(\theta)-\frac{G}{L_g}\ln\left(\frac{L_g\theta}{a^*\theta_0}\right),\end{aligned} \tag{18}$$

where

$$\gamma(\theta_0)=\left(\gamma_0+\frac{\epsilon(n_b)}{a_x}\right)\cos\theta_0, \tag{19}$$

and

$$a^*=a_x\exp(\epsilon_e/G). \tag{20}$$

Eq. (18) is precisely Marchenko's [10] result in the EDL if G can be identified as

$$G=2\frac{(1-\nu^2)\mathbf{F}^2}{\pi E}, \tag{21}$$

in which $\mathbf{F}$ is the surface force monopole acting at the ends of the bunch. Now, an expression for G was given in Eq. (10) in terms of $\mathbf{f}$, the strength of the vector surface dipole force at a step. To connect $\mathbf{F}$ with $\mathbf{f}$, note that the surface force density due to an array of steps with density $n(x)$ is given by

$$\mathscr{F}(x)=\int\mathbf{f}\delta'(x-x_0)n(x_0)\,dx_0=-\mathbf{f}\frac{dn(x)}{dx}. \tag{22}$$

$\mathscr{F}(x)$ can be integrated to obtain the force $\mathbf{F}$ on the surface at the edge of a bunch. Noting that the step density has a discontinuity of size n_0, where $n_0=(1/a_x)$ is the uniform step density in a bunch, we obtain

$$\mathbf{F}=\mathbf{f}\int\frac{dn(x)}{dx}\,dx=\frac{\mathbf{f}}{a_x}. \tag{23}$$

This result proves the equivalence of Eq. (21) to Eq. (10), and demonstrates that our theory is in

fact a microscopic version of Marchenko's[7]. In addition to connecting the surface force to the strength of the force dipole at the step, Eq. (20) gives a microscopic interpretation to the phenomenological edge energy, ϵ_e, in the Marchenko theory. Explicitly, in terms of the microscopic step interaction strengths, $\epsilon_e = U - 1.577G$.

Minimizing γ_g with respect to L_g at fixed θ and θ_0 gives

$$L_g = ae^* \frac{\theta_0}{\theta}, \tag{24}$$

which is identical to Marchenko's result in the EDL. At this minimum, we have

$$\gamma_g(\theta) = \gamma_0(\theta) - \left[\frac{G}{ea^*}\right]\frac{\theta}{\theta_0}. \tag{25}$$

To understand further the grooved configuration, we make use of the relations $L_g \sin\theta = L_1 \sin\theta_0$ and $L_g \sin(\theta_0 - \theta) = L_2 \sin\theta_0$ to show that

$$\gamma_0(\theta) = \cos\theta\left[\gamma_0 + \frac{\epsilon_\infty}{a_x}\frac{\tan\theta}{\tan\theta_0}\right]. \tag{26}$$

The full projected free energy for small θ and θ_0, is given by

$$f_g(\theta) = \frac{\gamma_g(\theta)}{\cos\theta} = \gamma_0 + \left[\frac{\epsilon_\infty}{a_x} - \frac{G}{ea^*}\right]\frac{\theta}{\theta_0}. \tag{27}$$

The contributions to the projected free energy for higher powers of θ/θ_0 come from bunch–bunch interactions that are ignored in the EDL.

For completeness we now compute the energy per step in a bunch without making the EDL approximation. We will show that this leads to Marchenko's full result, once again confirming that our model is identical to Marchenko's model at $T = 0$.

The key is to fully include bunch–bunch interactions, which contribute to the energy per step an amount

$$\Delta_e = G\frac{1}{n_b}\sum_{n=1}^{\infty}\sum_{i=1-n_b}^{n_b-1}\frac{n_b - |i|}{(nL_g/a + i)^2}, \tag{28}$$

where the geometry is again as illustrated in Fig. 3. Note that we assume, as did Marchenko, that $\theta \ll 1$ and $\theta_0 \ll 1$, but place no restrictions on the ratio θ/θ_0. In the dilute limit, where $n_b \gg 1$ and $L_g/a \gg 1$, but $n_b a/L_g$ is finite, the sum over i in the above can be evaluated by conversion into an integral. The result is

$$\Delta_e = -\frac{G}{n_b}\sum_{n=1}^{\infty}\ln\left(1 - \frac{n_b^2 a^2}{n^2 L_g^2}\right). \tag{29}$$

Adding Δ_e to the interaction energy from the bunch itself, we obtain (see Eq. (15))

$$\epsilon(n_b) = \epsilon_\infty + \frac{\epsilon_e}{n_b} - \frac{G}{n_b}\ln n_b - \frac{G}{n_b}\ln\left[\prod_{n=1}^{\infty}\left(1 - \frac{n_b^2 a^2}{n^2 L_g^2}\right)\right]. \tag{30}$$

$$= \epsilon_\infty + \frac{\epsilon_e}{n_b} - \frac{G}{n_b}\ln\left[\frac{L_g}{a}\,C\left(\frac{\theta}{\theta_0}\right)\right], \tag{31}$$

where we note that $n_b a/L_g \approx \theta/\theta_0$, and

$$C\left(\frac{\theta}{\theta_0}\right) \equiv \frac{\theta}{\theta_0}\prod_{n=1}^{\infty}\left(1 - \frac{1}{n^2}\frac{\theta^2}{\theta_0^2}\right) = \frac{1}{\pi}\sin\left(\frac{\pi\theta}{\theta_0}\right). \tag{32}$$

Eq. (31) is precisely Marchenko's result.

Using Eq. (31) in Eq. (19) and repeating the procedures used to obtain Eq. (24), we find that

$$L_g = \frac{\pi e a^*}{\sin(\pi\theta/\theta_0)}, \tag{33}$$

and

$$\gamma_g(\theta) = \gamma_0(\theta) - \frac{G}{\pi e a^*}\sin\left(\frac{\pi\theta}{\theta_0}\right). \tag{34}$$

Using Eq. (33) in Eq. (17) we find that, for small values of both θ and θ_0, the bunch size given by

$$n_b = 0.561\exp\left(\frac{U}{G}\right)\frac{\pi\theta/\theta_0}{\sin(\pi\theta/\theta_0)}, \tag{35}$$

[7] In Appendix A, by deriving an expression for G for a general anisotropic solid, we show that this connection holds for all crystalline interfaces.

depends not only on the ratio of attractive to repulsive interactions but also on the miscut angle, θ. With increasing θ, the bunch size monotonically increases from its value in the EDL given by Eq. (16). For small θ/θ_0, the result of Eq. (34) is equivalent to

$$f_g(\theta)=\frac{\gamma_g(\theta)}{\cos\theta}=\gamma_0+\left[\frac{\epsilon_\infty}{a_x}-\frac{G}{ae^*}\right]\frac{\theta}{\theta_0}+\left[\frac{G\pi^2}{6ea^*}\right]\frac{\theta^3}{\theta_0^3}, \tag{36}$$

a result that we shall need in Section 4.2. This result may also be obtained by a straightforward computation assuming that the bunches behave as point objects that interact via an inverse square interaction of strength Gn_b^2.

3.2. Phase diagram for $T>0$

At finite temperatures, it becomes favorable to form kinks in the steps for entropic reasons. This causes the steps within a bunch to fluctuate from their mean positions, leading to a decrease in the free energy. On general physical grounds then, we expect the free energy per step in larger bunch sizes to decrease less rapidly compared with smaller bunches as steps within larger bunches will have their fluctuations more constrained. If this happens, the free energies of smaller bunches will fall below those of larger bunches. We then expect larger bunches to rearrange themselves into smaller bunches, with increasing temperature, until eventually at very high temperatures only one step is left in the bunch. In this section, we show that this indeed happens.

Following the notation introduced for $T=0$, we write the energy per boson as

$$\frac{E_0[N,T,n_b]}{N}=\eta(T)+f(n_b,T)+O((N/L)^2), \tag{37}$$

where in the EDL, the bunch size n_b is obtained by minimizing $f(n_b,T)$, which is the contribution to the energy arising from interactions within a bunch. It is obtained by solving for the ground state energy of the Hamiltonian given in Eq. (11) for n_b bosons. For convenience, we introduce the scaled couplings

$$g\equiv G/t \text{ and } u\equiv U/t. \tag{38}$$

We illustrate our results in Fig. 4 for $U/G=u/g=1.65$. Here the energy per boson is plotted as a function of inverse temperature $g=G/t$ for $n_b=2$, 3 and 4. At low temperatures ($g>6.8$), the energy per boson in the 3-bunch has the lowest value, while at moderate temperatures ($6.8>g>4.54$) the 2-bunch gives the lowest energy per boson, while at high temperatures ($g<4.54$) the 1-bunch has the lowest energy (the 1-bunch becomes stable when $f(2,T)=0$). By repeating this procedure for $1\leqslant u/g\leqslant 3$, we have computed phase boundaries, shown as the solid curves in Fig. 5, for transitions from 1-bunch to 2-bunch, from 2-bunch to 3-bunch, and from 3-bunch to 4-bunch.

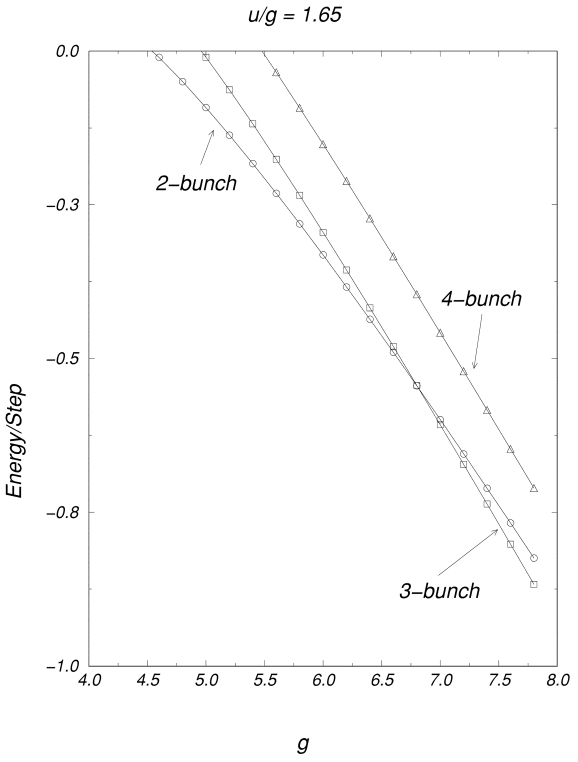


Fig. 4. Energy/step in bunches of size 2 (circle), 3 (square) and 4 (triangle) for $u/g=1.65$, plotted as a function of g. The energies are obtained by exact diagonalization of the quantum bunch problem on 12 sites in the case of 3- and 4-bunches and 200 sites for the 2-bunch.

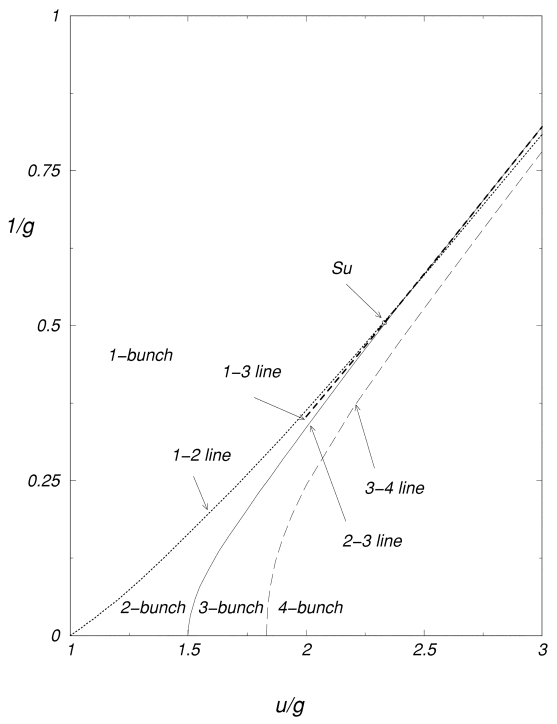


Fig. 5. Phase diagram in the EDL plotted in the u/g–$1/g$ space. The lines separate regions with stable bunch sizes that differ by one. The stable bunch size in each region is indicated in the figure. The 1–2 line (dotted line) lies above the 1–3 line (short-dashed line) for $u/g<2.4$, while lies beneath it for $u/g<2.4$. For $u/g>2.4$ the 1–3 line lies in between the 1–2 and 2–3 (solid line) lines. This implies that for $u/g>2.4$, the 1-bunch phase directly undergoes a transition to the 3-bunch phase bypassing the 2-bunch phase. The long-dashed line is the 3–4 line.

A key feature of plots shown in Fig. 4 is that the energy curves for bunches that differ in size by one intersect with a finite slope. This means that the derivative of the free energy of the vicinal surface with respect to temperature, or the entropy, is discontinuous at the transition, implying that the transitions are first order in the EDL. In the next section we will argue that, when bunch–bunch interactions are taken into account, the discontinuity in slope can vanish and the transition becomes continuous.

In order to obtain the phase boundaries between the n_b-bunch phase and the n_b-1-phase for a fixed u/g, one has to find the value of g that satisfies the equation $f(n_b, T)-f(n_b-1, T)=0$. We have done this numerically by using a standard root finding algorithm which approaches the root iteratively[8]. The root finding algorithm requires repeated evaluation of $f(n_b, T)-f(n_b-1, T)$ using exact diagonalization of the n_b and n_b-1 bunches for different values of g.

In calculating the energy of the 3-bunch and 4-bunch, we confined the bosons to 12 sites, while for the 2-bunch, 200 sites. In all the cases periodic boundary conditions were used which is also equivalent to arranging the sites around a ring. The ring sizes that we have used are sufficient to get accurate answers because the bunches are tightly bound with a mean particle spacing between 1 and 1.5, so that as long as the ring is bigger than about twice the bunch size, the energies do not change much. We have also computed the ground state energies using the Green's function Monte Carlo (GFMC) method for bunches confined on lattices with up to 100 sites and verified that the energies plotted in Fig. 4 are accurate. In Fig. 6 we show the energies computed for a 3-bunch on 12 sites using exact diagonalization and on 30 and 100 sites using GFMC (see Section 6 for details on GFMC simulations). For completeness, we have computed the mean particle spacing for the 3-bunch along the phase boundary separating the 2-bunch and 3-bunch regions and for the 4-bunch along the phase boundary marked between the 3-bunch and 4-bunch regions (see Fig. 5). These spacings vary from about 1.3 to 1.6 lattice spacings as u/g is varied from its values at the transition onsets up to $u/g=3$. It is clear that the bunches are very tightly bound in all the cases.

It is of considerable interest to understand how the limit $g\to 0$ is approached for our model. This limit, where only a near-neighbor interaction remains, has an exact solution (see, e.g. Refs. [11,24]) involving a first-order phase transition from a gas (infinitely dilute) of 1-bunches to a condensed phase (an ∞-bunch). Note from Fig. 5 that the 2–3 boundary crosses the 1–2 boundary at $u/g=2.4$ so that a 2-bunch is no longer stable for $u/g>2.4$. We also show the 1–3 transition line extending from $u/g=2$ upwards. This line cannot be distinguished from the 2–3 line for $u/g>2.4$,

[8] Details of this method can be found on page 258 of Ref. [23].

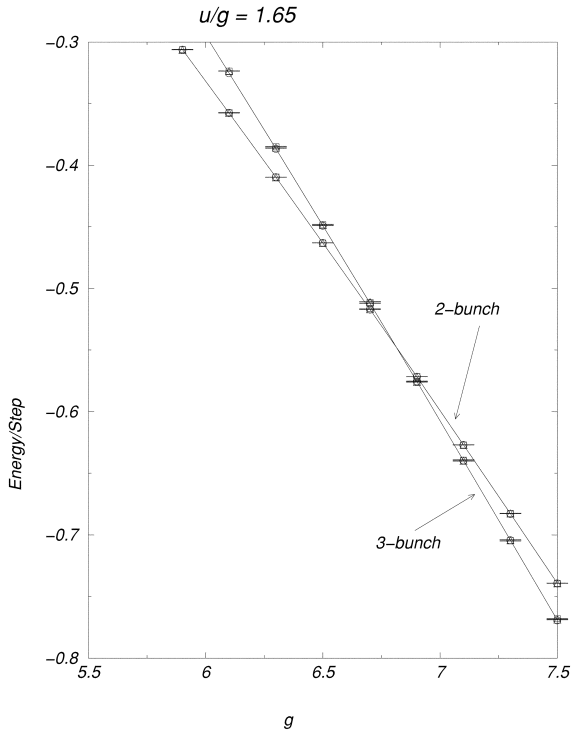


Fig. 6. Comparison of the exact diagonalization calculations and GFMC simulations. The circles indicate the energy per step in a 3-bunch confined to 12-sites and for a 2-bunch on 200 sites as found from exact diagonalization, while the triangles and squares represent the results for the 2-bunches and 3-bunches on 30 sites and 100 sites, respectively, as found using GFMC. The error bars on the GFMC energies are shown in the figure. Lines are drawn through the points to guide the eye. The slopes of the lines for the 2-bunch and 3-bunch phases are -0.268 and -0.315 respectively.

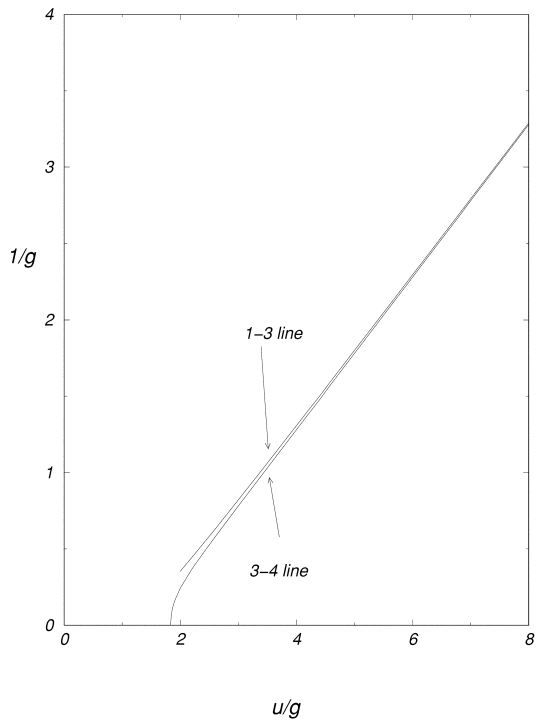


Fig. 7. Plot of the 1–3 line and 3–4 line for $u/g<8$.

but in fact lies slightly below it and above the 1–2 line. Thus, for $u/g>2.4$ in Fig. 5 the 1-bunch goes directly to the 3-bunch and then subsequently to the 4-bunch as the temperature or $1/g$ is lowered at fixed u/g. Further computation for values of u/g up to 8, depicted in Fig. 7, reveals that the 3–4 line comes very close to the 1–3 line while remaining below it. We then conjecture that as $g\to 0$ the $n-1$ transition lines become asymptotically equal for arbitrarily large n. This is clearly an approach to the $1-\infty$ transition, which is the first-order transition in the pure short-ranged potential case. As the transition in the short-ranged case is at $u=2$ [11,24], the asymptotic slope of the transition lines should be at $(1/g)/(u/g)=1/2$. This is indeed the case as seen in Fig. 7.

4. Phase diagram in the dilute limit

We will now consider the effect of the bunch–bunch interactions that were ignored in the previous section. We adopt the following steps in discussing this effect. (1) Using the general principles of quantum mechanics, we argue that when the inter-bunch interactions are turned on, the first-order transition should become continuous. (2) We then develop a perturbative approach to compute the free energy to $O(N/L)^3$ in the region where the inter-bunch interactions are small. (3) Finally, we estimate the regions around the first-order transition lines (obtained in the previous section) where the inter-bunch interactions become important. In the next section, we will then present the results of GFMC simulations on larger systems and show them to be consistent with our simple

theory. In particular we compute the 2-point correlation function, which clearly shows the bunching transitions in large systems.

4.1. General arguments

The effects of interactions on the bunches at $T>0$ can be understood qualitatively using arguments based on general principles of quantum mechanics. We confine our discussion to those regions in the phase diagram where the phase boundary between the n_b-bunch and the n_b-1-bunch phases is well separated from all the other phase boundaries. Consider Fig. 8, where we schematically plot the free energy per step in bunches of size n_b and n_b-1 as a function of the inverse effective temperature g for some fixed value of u/g. This is similar to Fig. 4, which was used to study phase transitions in the EDL. In this figure, we identify three regimes, namely, (1) regions where the free energy per boson in the n_b-bunch is much lower than the n_b-1-bunch, (2) regions where the free energies per boson in both the n_b-bunch and the n_b-1-bunch have comparable values and (3) the regions where the free energy of the n_b-1-bunch is much lower than that of the n_b-bunch. In regions (1) and (3) the ground state energy of a system with large number of bosons can be estimated using perturbative methods. Here to leading order the energy of the system is the energy of a bunch times the total number of bunches. The next to leading order comes from the bunch–bunch interactions via an inverse square interaction. In region (2), called the 'critical region', the physics is more complicated, since the system has nearly the same energy in both the n_b- and n_b-1-bunch phases. In this case we expect a splitting of the energy levels as sketched in Fig. 8, where the degeneracy of the energy levels is shown to be lifted as a result of bunch–bunch interactions. The extent of the region with significant splitting is denoted by $\Delta g(n_b \to n_b-1)$. This width, which vanishes in the limit of vanishing densities, can be written as

$$\Delta g(n_b \to n_b-1) \sim \Delta T_c(n_b \to n_b-1) \sim s^{p_{n_b}}, \qquad (39)$$

where $\Delta T_c(n_b \to n_b-1)$ is the width, in temperature, of the critical region and the exponent $p_{n_b}>0$ will be computed later in this section by comparing the free energies of the bunches of size n_b and n_b-1, derived perturbatively. The physics in the critical region is of general interest, and its relevance goes well beyond the problem we are studying. It involves coupling of modes with very different length scales. A tightly bound n_b-bunch in region (3) can be thought of as having excitations involving all the bunches as well as excitations within the bunch. While the wavelength of the former type of excitations is large (of the order of bunch spacing s^{-1}), the latter modes are localized in regions of the order of few lattice spacings. A bunch of size n_b-1 in region (1) will also possess similar excitations on both large and small scales. While the couplings between the excitations on different scales are small in regions (1) and (3), we expect strong coupling between the short and long wavelength modes in the critical region.

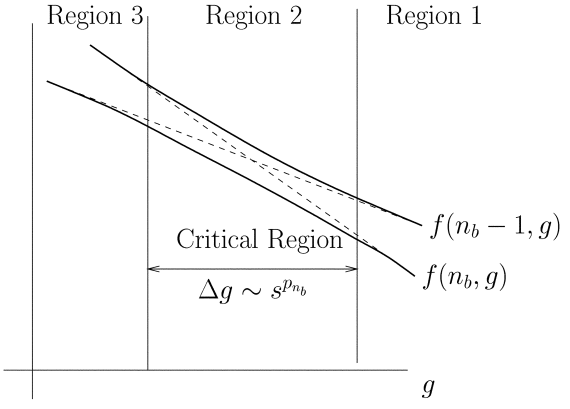


Fig. 8. Schematic plot of the free energy per step (solid curves) when the bunch–bunch interactions are taken into consideration. The dotted lines indicate the free energy per step in the EDL. In Region 1, the n_b-bunch has lower free energy while in Region 3 the n_b-1-bunch is lower in free energy. In the critical region, the free energy per step smoothly passes from $f(n_b, T)$ to $f(n_b-1, T)$. The width of the critical region indicated in the figure is estimated in the text.

4.2. Perturbative treatment for stable bunches

In order to compute the bunch–bunch interaction energy in regions with stable bunch sizes (such as regions (1) and (3) in Fig. 8), we make the following assumptions. (1) If a bunch has n_b

steps, then the stiffness of a bunch is $\Sigma_b = n_b\Sigma$, where Σ is the single bunch stiffness in the continuum limit. (In the discrete model, the kink energy required to make a kink in the bunch becomes $n_b\Sigma$. However, taking the appropriate limit of vanishing a_y would guarantee that the combination $\exp(-\beta n_b\Sigma)/a_y$ would scale as n_b). In making this approximation, we have ignored the contribution to the bunch stiffness that arises from interactions of the steps in the bunch. This is justified by the fact that average spacing in a bunch, for $u/g < 3$, remains well under two lattice spacings, so that the steps in a bunch remain tightly bound as a single entity. The approximation will be less accurate if the step spacing in the bunch is large, in which case bending of steps would also alter the interaction energy within the bunch. (2) The bunches interact with each other with a renormalized inverse square potential of strength $g_b = n_b^3 g$. This approximation is justified by noting that, in the dilute limit, the spacing between the bunches is very large, so that one bunch sees other bunches as if they were single lines without any internal structure. We note that the contributions to the energy of the system arising from the short range bunch–bunch interactions are smaller than the inverse square contribution by a factor proportional to the density of steps $s \ll 1$. This can be shown very easily using a Hartree–Fock estimation of the short-ranged contribution[9]. The energy of the system can then be computed using the Calagero–Sutherland model of hard-core bosons interacting via an inverse square law, for which an exact solution was provided by Sutherland [25]. Using his solution, we can write the energy per site in a system with bunches of size n_b as

$$\frac{E_0[s, T, n_b]}{L} = \frac{[\eta(T) + f(n_b, T)]a_x}{a_z}\, s + \left(\frac{\pi^2 (k_B T)^2 \lambda_b^2 a_x}{6 n_b^4 a_z^3 \Sigma}\right) s^3 + O(s^4), \quad (40)$$

where

$$\lambda_b = \frac{1}{2}\left[1 + \sqrt{1 + 2n_b^3 g}\right]. \quad (41)$$

[9] See Eqs. (8) and (9) of Ref. [11] for a derivation of this result.

An important point to make at this juncture is that in the limit of zero temperature, for large n_b, Eq. (40) is identical to Marchenko's result given in Eq. (36). It is then clear that Eq. (40) is the finite temperature extension of Marchenko's result, to order s^3.

4.3. Analysis of the critical region

In the critical region, since the energies of both the n_b and $n_b - 1$ bunches are nearly equal, we retain the terms of order s^3 arising from bunch–bunch interactions. In order to estimate the width of the critical region, we use the criterion $E(s, T, n_b - 1) \approx E(s, T, n_b)$, to obtain

$$s^2 \sim |f(n_b, T) - f(n_b - 1, T)|. \quad (42)$$

If

$$|f(n_b, T) - f(n_b - 1, T)| \sim |\Delta g(n_b \to n_b - 1)|^{\alpha_{n_b}}, \quad (43)$$

we obtain the result $p_{n_b} = 2/\alpha_{n_b}$, for p_{n_b} introduced in Eq. (39). For all the transitions from the 4- to 3-bunches as well as for the transitions from the 3- to 2-bunches, we see that the curves for the energy per step intersect with a finite slope for the parameter range that we have studied. This means that for these first-order transitions $\alpha_4 = \alpha_3 = 1$, the width of the critical region scales as

$$\Delta T_c \propto s^2. \quad (44)$$

For the unbinding of the 2-bunch to the 1-bunch, we find, for $g < 3/2$, $\alpha_2 = 2/\sqrt{1 + 2g}$, while for $g > 3/2$, $\alpha_2 = 1$, from which one can infer that

$$\begin{aligned} \Delta T_c(2 \to 1) &\propto s\sqrt{1+2g}, & g < 3/2, \\ &\propto s^2, & g \geq 3/2. \end{aligned} \quad (45)$$

As noted earlier the 3-bunch to 1-bunch transition pre-empts the 2-bunch to 1-bunch transition for $g < 1.86$. The 3-bunch to 1-bunch transition was seen to be first order in the entire range investigated.

Note next that the simplest conjecture for the shift of the transition temperature due to interactions is that it is of the same order of magnitude as the level shift given in Eq. (39). Explicitly, for

the transitions that are first order in the EDL,

$$|T_c(n_b \to n_b'; s) - T_c(n_b \to n_b'; 0)| \propto s^2. \quad (46)$$

While we find that all the transitions in the model are first order in the EDL, it is interesting to compute the shift in transition temperature for the 2-bunch to 1-bunch transition temperature when $g<3/2$. With our conjecture, and using Eq. (45) for $g<3/2$, one obtains

$$|T_c(2 \to 1; s) - T_c(2 \to 1; 0)| \propto s\sqrt{1+2g}. \quad (47)$$

Note that for this case our conjecture indeed yields the result derived within continuum theory [7,8] using renormalization group methods.

While we have used simple arguments to predict the width of the critical region and the shift of the transition temperature, a detailed analysis of the nature of unbinding transitions and the form of the free energy require further study of the many-body problem involving the thermodynamic limit. One natural way to study this is by means of computational methods such as GFMC or exact diagonalization methods for large systems. In the following section, we discuss the results obtained using GFMC simulations.

5. Quantum Monte Carlo simulations

In the preceding section we argued, on the basis of results for the *extreme* dilute limit from exact diagonalization of small systems, that the bosons undergo bunching transitions as strengths of the interaction parameters are varied. In this section, we will perform calculations on larger systems to study directly the dilute limit and to attempt to understand the physics in the 'thermodynamic limit'. In addition to exact ground state energy, we also study pair correlation functions in order to probe the structure of the many-body state, in particular the occurrence of bunching and transitions between different bunch sizes.

The primary method we use is the Green's function Monte Carlo (GFMC) method [26,27], a Monte Carlo method to study ground state properties of quantum many-body systems which is exact for bosons. Variational Monte Carlo (VMC) calculations are performed prior to GFMC, in order to optimize our variational wave function, which is used to generate the initial state and also as the importance function in GFMC. In Appendix C, we present a brief self-contained treatment of these methods. The algorithm we use follows closely that of Refs. [28,29], which we refer the reader to for more details.

The variational many-body wave function used is of the Jastrow form, written as a product of two body correlations, i.e.

$$\psi_T(x_1, x_2, \cdots, x_N) = \prod_{(i,j)} f(|x_i - x_j|), \quad (48)$$

where $|x_i - x_j|$ is the mean distance between particle i and particle j. The function $f(r)$, where r is a positive integer, is chosen to be of the form

$$\begin{aligned} f(r) &= a(r-r_0)^2 + d, && r \le r_0, \\ &= 1 - \frac{f_2}{r^\alpha} + b\exp(-cr), && r > r_0, \end{aligned} \quad (49)$$

Defining $f(1) \equiv f_1$, we choose $f_2 = (\alpha + r_0)\, x r_0^{\alpha-1}(1-d)$, $c = 1 + \alpha/r_0$, $b = \alpha f_2 \exp(cr_0)/cr_0^{\alpha+1}$ *and* $a = (-d+f_1)/(1-r_0)^2$, thus reducing our variational parameters to four, namely, f_1, r_0, d and α. We note that the parameters are chosen such that $f(r)$ and $\mathrm{d}f/\mathrm{d}r$ at $r = r_0$ are continuous. These parameters have direct physical implication as shown in Fig. 9.

In both the VMC and GFMC, we used 500 walkers (on the average for GFMC) for computing the averages. In the variational calculation, measurements were made after 10 000 metropolis steps. In the GFMC calculations measurements are made after 100 000 steps during which the system relaxes from the initial variational distribution. Measurements were made for a total of 200 000 steps, and statistical errors were obtained by dividing these into 200 blocks of 1000 steps each and estimating the variance of the block measurements.

We present results for three separate cases, namely, $u/g = 1.25$, 1.65, 2.0. These cases are chosen so that in the limit of $g \to \infty$ the ground states have bunches of size 2, 3 and 4 bosons, respectively.

First we show in Table 1 a comparison of GFMC and exact diagonalization results for the

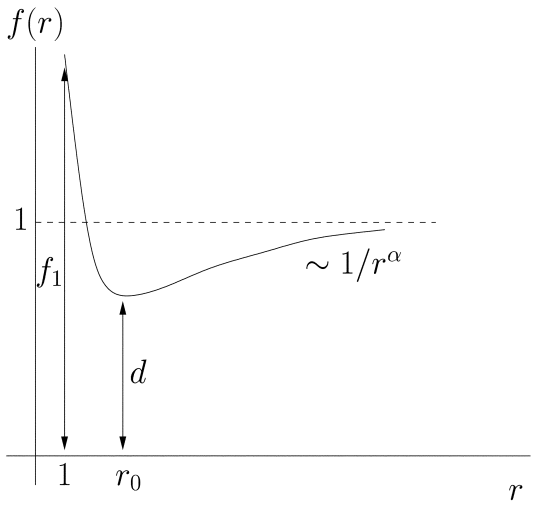


Fig. 9. Schematic depiction of the two body correlation $f(r)$ used in the trial wave-function. The function $f(r)$ takes on a value f_1 at $r=1$ has a minimum value of d at $r=r_0$ and behaves as $1-\text{const}/r^{\alpha}$ for large r.

energy of a small system of three bosons. In the exact diagonalization the bosons are confined on 12 sites in a ring, i.e. with a periodic boundary condition. The results are shown together with those from GFMC for the same system. The agreement is exact. This is to be expected, since GFMC yields exact ground state energies. Also shown are the energies computed by GFMC for a ring of size 30 and 100 respectively. We see that they are indistinguishable from the corresponding results for 12 sites, indicating that at 12 sites the finite-size effect is already negligible. This confirms our earlier conclusion that the three bosons are tightly bound. In Fig. 6, we again compare GFMC results for 2- and 3-boson systems on 30 sites with our exact diagonalization results, over a wider range of parameter space. The excellent agreement reassures that our GFMC code is well-behaved, and that the small system sizes used in exact diagonalization calculations of the EDL are justified.

In Tables 2–4 we present the variational wavefunction and the energies E_{VMC} and E_{GFMC} and compare them with the approximate energy E_{approx} of the Hamiltonian given by Eq. (11). (For clarity we do not include the first term which is proportional to the number of bosons, since it does not directly affect the physics of bunching transitions.) For N bosons on L sites, E_{approx} is computed from the energy per boson $f(n_{\text{b}}, T)$ computed using exact diagonalization and the approximate interaction energy using

$$E_{\approx} = \frac{Nf(n_{\text{b}}, T)}{n_{\text{b}}} + \frac{\pi^2 \lambda_{\text{b}}^2 N^2}{3n_{\text{b}}^4 L^3}, \tag{50}$$

where λ_{b} is given by Eq. (41). In computing E_{approx}, the value of n_{b} is obtained from the phase diagram given in Fig. 5. For all the values of u/g, for large g, we see that there is good agreement between the GFMC and approximate energies and fair agreement for small values of g. These results confirm the approximations made in the analysis of bunching and bunch–bunch interactions. As g is decreased, the system is more quantum mechanical and each bunch is less tightly bound, hence E_{approx} becomes worse. Note that in all the cases $E_{\text{GFMC}} < E_{\text{approx}}$, which is not surprising since we did not consider the role of the short-range attraction between the bunches in evaluating E_{approx}.

We also calculate the pair correlation function

Table 1
Comparison of the exact diagonalization and GFMC results for three bosons confined on 12 sites with $u/g=1.65$. E_{exad} denotes the energy per boson obtained by exact diagonalization, E_{var} is the variational energy per boson on 12 sites and E^{12}_{GFMC} represents the GFMC result. The number bracket, corresponding to the GFMC energies, indicates the error on the last decimal place. In all the cases a variational wavefunction with $r_0=3$, $f_1=1.14$, $d=0.5$ and $\alpha=0.6$ was chosen. We also give the GFMC energies, E^{30}_{GFMC} and E^{100}_{GFMC}, for three bosons occupying 30 and 100 sites respectively

g	E_{exad}	E_{VMC}	E^{12}_{GFMC}	E^{30}_{GFMC}	E^{100}_{GFMC}
6.5	−0.44902	−0.34(3)	−0.4489(2)	−0.4490(4)	−0.4492(7)
6.9	−0.57562	−0.47(3)	−0.5756(1)	−0.5756(4)	−0.5753(6)
7.3	−0.70425	−0.63(4)	−0.7042(1)	−0.7043(4)	−0.7046(6)

Table 2
Energies for $u/g=1.25$ and values of g shown in the table, computed for 10 bosons on 100 sites. The variational energy is denoted by E_{VAR}, the GFMC energy by E_{GFMC} and E_{approx} is the approximate energy computed using Eq. (50). The variational wave function parametrized by r_0, f_1, d and (see Eq. (49)) is also tabulated

g	r_0	f_1	d	α	E_{VMC}	E_{GFMC}	E_{approx}
10.0	2.0	1.05	0.58	1.5	3.63(4)	2.312(1)	3.071
12.0	2.0	1.06	0.58	1.5	3.76(5)	2.221(1)	3.553
15.0	2.0	1.06	0.30	0.5	2.37(6)	−0.479(1)	−0.424
20.0	2.0	1.14	0.18	0.5	−0.10(1)	−6.701(2)	−6.223

Table 3
Energies for $u/g=1.65$ and values of g shown in the table, computed for 12 bosons on 120 sites. The symbols have same meanings as in Table 2

g	r_0	f_1	d	α	E_{VMC}	E_{GFMC}	E_{approx}
3.0	4.0	1.02	0.7	1.0	1.99(2)	1.139(1)	1.311
4.0	4.0	1.02	0.3	0.4	1.85(4)	1.032(1)	1.579
5.0	4.0	1.02	0.4	0.4	0.40(3)	−0.620(1)	−0.486
6.0	4.0	1.14	0.1	0.1	−1.68(9)	−3.340(3)	−3.363
7.5	4.0	1.14	0.1	0.1	−6.83(7)	−8.870(7)	−8.742
15.0	4.0	1.16	0.1	0.1	−33.77(3)	−39.075(3)	−38.814

Table 4
Energies for $u/g=2.0$ and values of g shown in the table, computed for 12 bosons on 120 sites. The symbols have same meanings as in Table 2

g	r_0	f_1	d	α	E_{VMC}	E_{GFMC}	E_{approx}
2.25	3.0	1.04	0.7	0.7	1.11(1)	0.807(1)	1.104
2.85	3.0	1.06	0.5	0.1	0.89(1)	0.051(5)	0.119
2.96	4.0	1.02	0.1	0.1	0.34(2)	−0.301(1)	−0.209
3.5	4.0	1.02	0.1	0.1	−2.31(3)	−3.181(1)	−3.160
4.0	4.0	1.06	0.1	0.1	−4.61(1)	−6.165(5)	−6.144
7.0	4.0	1.06	0.1	0.1	−24.21(3)	−26.779(1)	−26.665

which for L even is defined as

$$g(x)=\frac{L}{2N^2}\left\langle \sum_{i\neq i'} \delta(x-x_i+x_{i'}) \right\rangle, \tag{51}$$

where $1<x<L/2-1$ and the brackets, $\langle\rangle$, indicate the quantum mechanical average in the ground state. In the expression for $g(x)$, x_i and $x_{i'}$ are the coordinates of the bosons i and i'. In writing Eq. (51), we have made use of the fact that the bosons are confined to a periodic ring.

In GFMC the mixed estimate is used to compute the average indicated in Eq. (51). Recall that the mixed estimate[26,27] for the expectation value of an operator $\mathcal{O}$ is

$$\langle \mathcal{O} \rangle_{mixed} = \frac{\langle \Psi_T |\ \mathcal{O} | \psi_0 \rangle}{\langle \psi_T | \psi_0 \rangle}, \tag{52}$$

where $|\psi_0\rangle$ is the ground state wave function while $|\psi_T\rangle$ is the trial wave function. While exact for the energy, this estimator yields an approximate ground state expectation value for other operators. If $|\psi_T\rangle$ is good, a simple extrapolation [26,27] of the mixed estimate with the variational expectation can lead to a further improved result. Our $|\psi_T\rangle$ is relatively poor, giving variational estimates of $g(x)$ which are rather structureless in the long range,

so we did not attempt this extrapolation. However, as we see below, even with this $|\psi_T\rangle$, $g(x)$s computed from the mixed estimate clearly show the bunching structure.

For $u/g = 1.25$, Fig. 10 shows the pair correlation function for 10 bosons on 100 sites respectively. We see that for large g ($g=20$ and $g=15$), the pair correlation function shows two equal peaks near $x=20$ and $x=40$. Taking into account the periodic boundary condition, we see that this indicates the presence of five 2-bunches in the system. Note that the 2-bunch at $g=15$ is more loosely bound than the 2-bunch when $g=20$. When $g=10$ the system is a completely unbound state. The case $g=12$ is in the intermediate region, where the pair correlation still has a large peak at the nearest neighbor site, but does not show peaks at positions which indicate the presence of either a 1-bunch or a 2-bunch. This value of g corresponds to a value of the potential such that the system is in the critical region of the phase diagram. In this region the 2-bunch ground state continuously unbinds into one with single bunches.

We next consider the case $u/g = 1.65$, where we study the ground state of 12 bosons on 120 sites. Fig. 11 shows that for large g ($g=15$ and $g=7.5$) there is clearly a 3-bunch, which starts unbinding at $g=6$. At $g=5$ there is a 2-bunch. This starts to unbind around $g=4$ to a single bunch ground state. It is clear that the cases $g=6$ and $g=4$ fall

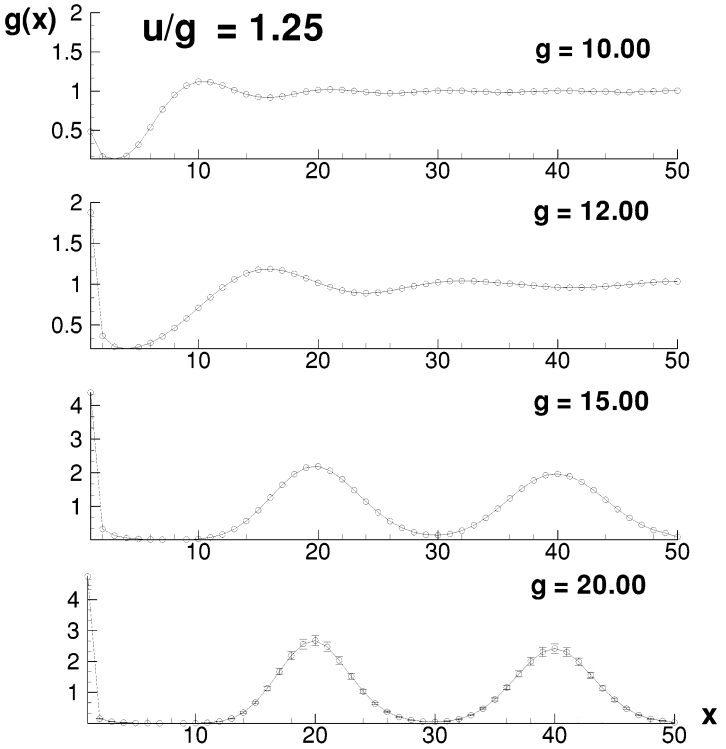


Fig. 10. The boson pair correlation function $g(x)$ for 10 bosons on 100 sites with $u/g=1.25$ for values of g indicated in the figure. The points are also marked in Fig. 13 for comparison. By counting the number of peaks in $g(x)$ and making use of the periodic boundary condition the number of bosons in a bunch can be established. For example, in the case $g=20$, there are two peaks at $x=20$ and $x=40$ in addition to a large value of $g(x)$ on the near neighbor site. Invoking the periodic boundary condition, one sees that, if there are two bosons in a bunch, the four peaks at $x=\pm 20$, $x=\pm 40$ account for eight bosons, which along with the boson on the near neighbor site and the boson at the origin add up to 10 bosons. For $g=20$ and $g=15$ we have a well-defined 2-bunch phase, while there is a well-defined 1-bunch phase for $g=10$. The figure shows that $g=12$ is in the critical region since here $g(x)$ lacks peaks associated with either 1-bunches or 2-bunches, instead having a peak at an intermediate position. We illustrate the statistical error bars only for the case $g=20$, since in all the other cases they have similar magnitudes.

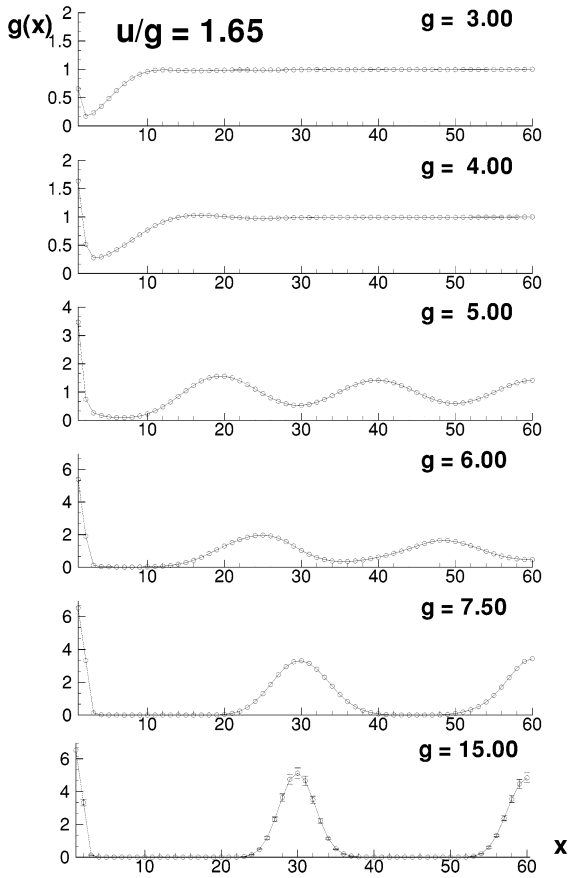


Fig. 11. Boson pair correlation function (Eq. (51)) for 12 bosons on 120 sites with $u/g=1.65$ for values of g indicated in the figure. The points are also marked in Fig. 13 for comparison. Counting the number of peaks as we did in Fig. 10 gives the number of bosons in a bunch. To account for the 3-bunches, note that when $g=15$ there are 2 peaks at $x=30$ and $x=60$ in addition to large values of $g(x)$ on the near neighbor and next to near neighbor sites. Invoking the periodic boundary condition, we see that the peaks at $x=\pm 30$ account for six bosons while the peak at $x=60$ accounts for three bosons which along with the boson at the origin and those on two adjacent sites account for all 12 bosons. For $g=15$ and $g=7.5$ we have a well-defined 2-bunch phase, while there is a well-defined 2-bunch phase for $g=5$ and 1-bunch phases for $g=4$ and $g=3$. The figure shows that $g=6$ is in the critical region. The statistical error bars for all values of g have about the same magnitude as the case $g=15$ where they have been explicitly displayed.

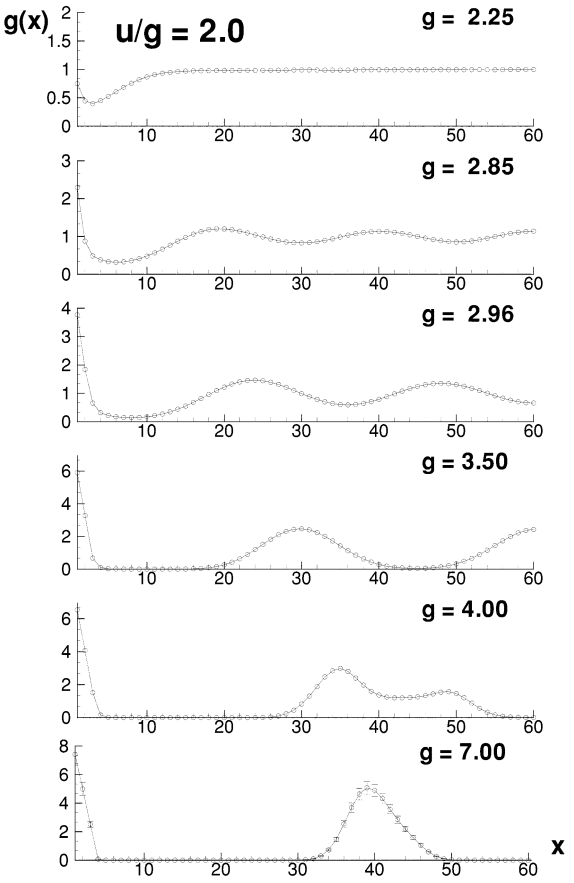


Fig. 12. Boson pair correlation function (Eq. (51)) for 12 bosons on 120 sites with $u/g=2.0$ for values of g indicated in the figure. The points are also marked in Fig. 13 for comparison. By counting the number of peaks in $g(x)$ as we did in the previous figures, we see that for $g=7.0$, $g=3.5$, $g=2.85$ and $g=2.25$ we have well-defined 4-, 3-, 2- and 1-bunch phases respectively, while the points $g=4$ and $g=2.96$ are in the critical region. The error bars have only been shown for the case $g=7$, since in all the other cases they have similar magnitudes.

in the critical region, where the unbinding of a 3- to 2-bunch ground state and 2- to 1-bunch ground state takes place, respectively. From Fig. 12, for $g=2$, it is evident that a 4-bunch first unbinds to a 3-bunch, then to a 2-bunch and finally a 1-bunch.

In Fig. 13, we show points corresponding to Figs. 10–12 on the phase diagram derived for the EDL. Since these points are for larger systems in the dilute limit, with multiple bunches present and interacting, the precise phase boundary locations for these systems are expected to differ from those for the EDL. We see that the behavior of the pairing correlation functions is completely consistent with the conjectured phase diagrams.

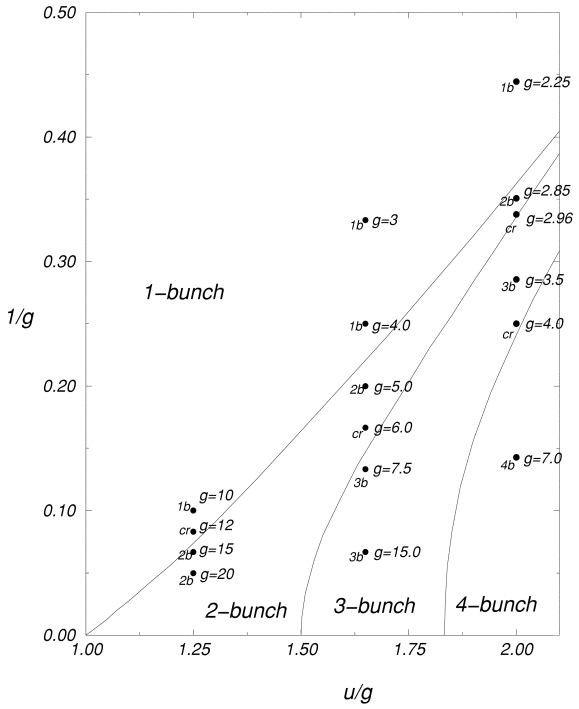


Fig. 13. Comparison of the phase diagrams obtained in the EDL using exact diagonalization and GFMC simulations. For $u/g=$ 1.25, 1.65, 2.0 the pair correlation functions for the marked values of g are given in Figs. 10–12. For each value of g we also indicate the bunch size (1b, 2b, 3b and 4b correspond to 1-, 2-, 3- and 4-bunches respectively, while cr refers to the critical region) obtained from GFMC simulations. Note that the GFMC results and the exact diagonalization results do not agree exactly since in the dilute limit the bunch interactions can alter the nature of the phases especially close to the phase boundaries.

6. Comparison of our theory with continuum theories

Recently the effect of competing short-range and long-range interactions on the finite temperature phase transitions on vicinal surfaces was considered by Lässig [7] and Bhattacharjee [8], who studied a continuum version of the model considered in this paper. In their model the steps interact via a short-range attractive part, modeled as a contact potential of strength $-u$ using an appropriate limiting procedure. They analyzed the phase transition using renormalization group (RG) techniques, finding a tricritical point and an associated first-order transition with coexisting bulk phases representing a flat facet and a vicinal surface with a non-zero step density vanishing with an interaction-dependent critical exponent as the tricritical point is approached. The continuum approach did not yield bunches of finite size, either the small bunches seen by Sudoh et al. [5,6] or the large bunches seen by Song et al. [1–3] and Yoon et al. [4]. Indeed, Lässig [7] specifically notes (in his footnote 26) that his model cannot obtain bunch sizes. A more realistic continuum theory, with the hard-core cut-off accounted for and a finite-range attractive portion, would presumably predict bunches similar to those in our lattice theory.

As noted earlier, the work of Bhattacharjee [8] has been extended by Bhattacharjee and Mukherji [9]. Here conjectures concerning some bunched phases are made in the context of three-body interactions. The relevance of the latter to the experimental systems of interest remains unexplored.

In our picture, the steps do not phase separate, except in the limit $U/G\to\infty$. Instead, the steps group themselves into bunches of a finite size. The bunches then fill the space and interact with each other with renormalized interaction parameters as discussed in the text. In the EDL, with increasing temperature the steps undergo a series of bunching transitions wherein the number of steps in a bunch decreases progressively. As mentioned earlier, the size of a bunch and the bunching transitions are lattice effects which are not present in the continuum model.

As noted in Section 1, the phase transitions observed at fixed slope by Song et al. [1–3] and Yoon et al. [4] are in the limit where the bunch size L_g becomes infinite ($\theta_0\to\theta$) in Eq. (33) and the relative spacing between bunches $L_2/L_g\to 0$. This limit is the opposite of the EDL and is a regime we are at present unable to treat explicitly. Nevertheless, since our model contains the continuum theory as a limit we expect that its critical properties near phase transitions for large bunches will be essentially the same as those of the continuum theory, where this theory applies.

For a fixed strength of the interaction, the continuum theory captures the onset of the phase

separation instability as the temperature is decreased. In our model, in the EDL, the first instability that is encountered on cooling from the high temperature phase is the point where 2-bunches first appear. For this transition, we find quantitative agreement with the continuum RG theory. In particular, the width of the critical region scales with density as

$$\Delta T_c(s) \propto s^{\sqrt{1+2g}}. \quad (53)$$

[7] for $g<3/2$, which is precisely the relation that we obtain in Eq. (47). For $g>3/2$, the continuum theory fails to make any predictions because of a singularity, but it was speculated that the transition becomes first order [7]. However, the natural cutoff present in the lattice model prevents such a problem.

7. Comparison of theory with experiments on silicon surfaces

As noted in Section 1, one of the objectives of this work is to elucidate the experimentally observed exponents and the physics of bunching phenomena. In principle, to accomplish this one would have to carry out the calculations detailed in the text using interaction potentials between steps derived from electronic structure or other quantum mechanical calculations. Since such calculations are not available at this time, we use the simple model with an attractive interaction restricted to only near neighbor sites to interpret the experimental observations.

7.1. Experiments of Song et al. and Yoon et al.

We first consider the experiments of Song et al. [1–3], where X-ray scattering studies were conducted on Si(113) miscut from the [113] direction towards [001]. It was seen that, depending on the slope of the miscut surface s, above a temperature $T_c(s)$, the surface is uniformly stepped, while the surface consists of flat (113) portions separated by step bunches below $T_c(s)$. From the measurements it was inferred that $s \sim |T_c(0)-T_c(s)|^\beta$, with $\beta = 0.42 \pm 0.1$. For fixed miscut slope s, the misorientation angle, or slope, s_m of the bunches increases as T is decreased below $T_c(s)$, tracing out the curve $T=T_c(s_m)$. Also, as the temperature is decreased below $T_c(s)$, both the number of steps in a bunch and the size L_g of the associated groove vary, passing through a minimum in a fashion embodied in the Marchenko results appearing in our Eq. (33) and Eq. (35). For the case of a miscut angle of 2.1°, n_b varies between about 24 and 31 [3]. Using Eq. (35), this corresponds to variations of U/G between 3.3 and 3.8. For the case of a miscut angle of 1.3°, n_b varies between about 13 and 20 [3]. Using Eq. (35), this corresponds to variations of U/G between 2.7 and 3.5. These variations in U/G reflect the dependence of ϵ_e/G on the misorientation angle θ_0 found in Ref. [3].

The observed decrease in n_b with decreasing miscut angle noted in the previous paragraph is expected from Eq. (35). It is interesting to consider the case of even smaller miscut angles. Note that the limiting value of n_b for $\theta \ll \theta_0$ is given by $n_b = ea^*\theta_0/a_z$. Using the measured values of a^* [3], this gives $n_b \approx 3\theta_0$, where θ_0 is given in degrees. This suggests that small, widely separated bunches can occur on Si(113) for $\theta \ll \theta_0$. As the EDL is the limit $\theta/\theta_0 \to 0$, this is just the case where our results are most applicable. We encourage experiments with smaller miscut angles.

The recent renormalization group calculations [7,8] predict that the exponent β depends on the ratio of the strengths of the attractive and repulsive interaction strengths. In the region where these calculations are valid, the exponent $\beta \geq 0.5$. The exponent $\beta = 0.5$ corresponds to a special point for 1D systems interacting via the inverse square potential, a point beyond which the renormalization group methods fail. The continuum theories therefore require a particular value for U/G to obtain agreement with experiments. The experiments of Yoon et al. [4] report results consistent with $\beta = 0.5$ for surfaces miscut in very different azimuthal directions. This calls into question the applicability of continuum theory here, as U/G would be expected to depend on the direction of miscut. Indeed, as seen from Eq. (20), the elastic length a^* is determined by U/G, and the experiments of Song et al. [3] and Yoon et al. [4]

demonstrate that a^* varies both with miscut direction and misorientation angle.

We note further that the step separations of Song et al. [2], since a sequence of nearest neighbor steps on a (113) facet corresponds to the (114) direction, amount to only 1–3 nearest neighbor distances. In this limit a continuum theory, valid for step separations large compared with step sizes is questionable, and a complete treatment must be lattice based.

All phase transitions studied in our lattice theory are first order in the EDL. Bunch–bunch interactions render them continuous as described by Eqs. (44) and (46). While we are unable to treat explicitly the case of large, strongly interacting bunches, we conjecture that the same physics holds. This provides a natural and robust explanation of the experimentally observed critical exponent $\beta \approx 0.5$. This scenario would imply that the sequence of bunching transitions observed in the EDL is washed out in the strongly interacting case, leaving a single transition. This is consistent with the experiments lying in a regime corresponding to $g > 3/2$ in the continuum theory, with the caveat that the first-order transition conjectured [7] for this region is rendered second order by bunch–bunch interactions.

An important point to make here is that, since bunch phases are single equilibrium phases distinct from coexisting macroscopic phases, the two-phase region predicted by the continuum theory is in fact a single-phase region. Further, the coexistence curve of Song et al. is not a conventional coexistence curve but a line of transitions, continuous in our picture, to a bunched phase. In fact, Marchenko [10] was the first to make this point in the context of crystal shapes.

7.2. Experiments of Sudoh et al.

We now turn to the recent experiments of Sudoh et al. [5,6] where the morphology of Si(113) surfaces, miscut towards a low symmetry azimuth which is 33° away from the $[\bar{1}10]$ direction to the $[\bar{3}\bar{3}2]$ direction was studied using scanning tunneling microscopy (STM). The authors compared surfaces quenched after annealing at various temperatures in the range 600–1000°C. Annealing at temperatures above 720°C resulted in single-, double-, and triple-height steps, while on annealing at temperatures in the range 690–720°C the average terrace spacing increased because of the presence of double-, triple-, and quadruple-layer steps. The sizes of the terraces saturate during annealing, indicating that the surface had reached local thermal equilibrium. STM images at 710°C show a predominance of double steps. The authors also find that the stiffness of a step is proportional to its height, with an additional stabilization of double-height steps.

It is possible to understand the approximate number of steps observed in Ref. [5] in comparison with the results of Song et al. Though the authors state that their overall miscut angle was $\theta = 1.7°$, the portion of the surface shown in their Fig. 1 shows a total of 21 steps in a length of 360 nm, corresponding to a local value $\sim 0.5°$. Since n_b (see Eq. (35)) decreases with decreasing miscut angle, we might expect smaller bunch sizes than for the Song et al. experiments, performed for $\theta = 1.3°$ and $\theta = 2.1°$ [10]. Indeed, for the typical angles θ_0 observed by Song et al. (Sudoh et al. do not provide values for θ_0), the relation $n_b \approx 3\theta_0$ noted in Section 7.1, gives n_b as small as 4. However, these estimates will begin to fail for such small values of n_b, and an analysis in terms of small-bunch phases is necessary. A possible scenario is given in the next paragraph.

We conjecture that the temperature around 720°C corresponds approximately to $u/g \approx 2.35$ and $1/g \approx 0.5$, where the stable phase is the 2-bunch phase. This point is marked as 'Su' in Fig. 5. Note that both the 1–2 line and 2–3 lines are very close to this point, while the 3–4 line is also nearby. This means the free energies of the 1-, 2- and 3-bunches are very close to each other with the free energy of the 2-bunch being the lowest, explaining its stability. Though the 2-bunch is stable in the EDL, the point Su is very likely to be in the critical region, where the 1- and 3-bunch phases are stabilized by bunch interactions. Further decreasing the temperature results in the

[10] This assumes weak dependence of n_b on miscut azimuth. In favor of this assumption we note that values of L_g are similar for the different azimuths of Refs. [3,4] and that of Ref. [5].

emergence of the 4-bunch phase, which can be understood by noting that the system then moves closer to the 3–4 line resulting in the stabilization of the 4-bunch owing to bunch interactions. We also point out our arguments that the stiffness of the bunched steps should be proportional to the number of steps in the bunch is also borne out in the experiments.

Step bunches with n_b in the range 1–4 have also been seen on miscut Si(113) by other workers, specifically van Dijken et al. [30] and Zhu et al. [31]. Equilibrium does not appear to have been achieved in these cases.

8. Discussion and future directions

In this paper we have explored the phase transitions arising in vicinal surfaces with competing long-range and short-range interactions. We showed that, depending on the strength of the interactions and the temperature, the steps on the surface rearranged themselves into bunches. Using a tractable model for step interactions, we showed that the bunch size increased with decreasing temperature through a series of bunching transitions. At $T=0$, we showed that the bunch phases predicted by our model correspond to the well known periodic groove structure first predicted by Marchenko. Our theory can then be considered as an extension of the Marchenko theory to finite temperatures, where changes in the size and number of steps in a groove are brought about by the bunching transitions. A simple conjecture concerning quantum level crossover, within the context of our model, provides a possible explanation of the observed exponent $\beta \approx 0.5$ describing the dependence of the phase transition curves of Song et al. and Yoon et al. on the misorientation angle. In contrast to the recent RG calculations that require a particular ratio of the attractive to repulsive interaction strengths to obtain $\beta = 0.5$, our analysis shows that this value of the exponent is robust, applying to all the bunching transitions that are first order in the EDL. We comment that the physics of bunching transitions we study here is very different from the recently studied step bunching due to applied stress, electromigration and other kinetic effects [32,33]. In our case, the bunching transitions occur in an equilibrium setting due to competing interactions acting on different length scales.

We now point out some further directions for future theoretical and experimental research that can provide more insights on equilibrium bunching on vicinal surfaces. On the theoretical/computational side, it is very important to have an accurate determination of the step interaction potential. This can be done through quantum calculations or atomistic simulations using reliable empirical inter-atomic potentials. Once the step interactions are known, the methods developed in this paper can be used to study the step bunching transitions. Further, a more detailed understanding of large, strongly interacting bunches would put our conjecture concerning quantum level crossover on a firm footing. On the experimental side more data on surfaces with competing interactions can shed light on the role of attractive interactions on equilibrium bunching properties. In particular for vicinal surfaces in a bunched phase, the crystal shape will exhibit a Pokrovsky–Talapov transition as the facet is approached. This is also true within the Marchenko picture. An experimental check of this feature would be valuable.

More detailed study of the step phases as a function of orientation of the silicon surfaces away from the [113] direction, and for smaller miscuts at fixed orientation, would be most useful in order to elucidate the connection between the experiments of Sudoh et al. and those of Song et al. and Yoon et al. Note that miscuts such as those in the former experiments introduce kinks in steps on the Si(113) surface. For low kink densities, the model parameters G, U, and η should have corrections proportional to the kink density. The phase boundaries in Fig. 5 will then shift linearly with kink density, providing a means of tuning the model parameters. For cases such as those marked by Su in Fig. 5, small changes in the kink density would lead to pronounced effects owing to the close proximity of phase boundaries.

The quantum n-bunch, or n-mer, phases discovered in this work are highly interesting in their own right, independent of their realization in crystal surface physics. While we expect these phases to be Luttinger liquids well away from transitions

from one bunch phase to another, the picture may change in the crossover region where there is a mixing of the long-wavelength modes associated with phonon-like oscillations of the bunches and the modes internal to the individual bunches. In effect, new many-body phases may emerge in the critical region. A detailed study of the crossover region will shed light on some of these new physical phenomena.

Acknowledgements

VBS would like to thank Sanjay Khare and Avraham Schiller for stimulating discussions. The Quantum Monte Carlo Simulations were performed on the IBM SP2 at the Ohio Supercomputer Center. VBS acknowledges the support of AFOSR-MURI program at Brown University. SZ is supported by the NSF under grant DMR-9734041 and by the Research Corporation.

Appendix A: Step interactions and connection to Marchenko's model in anisotropic crystals

For isotropic crystals, using the expression for elastic interactions between steps given by Eq. (10) and the energy of an array of force monopoles derived by Marchenko [10], in Section 3, we showed the equivalence of our lattice model to Marchenko's continuum model. In this appendix, we will first generalize Eq. (10) to include anisotropy and then derive an expression for the interaction energy of an array of force monopoles in anisotropic crystals. Using these results it will be shown that the equivalence of our lattice model to Marchenko's model holds for any crystalline solid.

Let us first define the anisotropic surface Green's function, $\mathscr{G}(x, z)$, that can be used to obtain the displacement $\mathbf{u}(x, z)$ due to a line force distribution $\mathscr{F}(\boldsymbol{x})$ acting on the surface through the relation

$$\mathrm{u}(x, z) = \int \mathscr{G}(x - x', z)\mathscr{F}(x')\,\mathrm{d}x'. \tag{A1}$$

Note that since the line force is of infinite extent in the y-direction, $\mathscr{G}$ does not depend on y. The anisotropic surface Green's function can be readily used to obtain the displacement fields of force monopoles and dipoles. While surface Green's function can only be evaluated in closed for isotropic crystals and for some very special orientations of anisotropic crystals [34], for any general orientation of a crystalline surface, we can use the approach proposed by Ting [35] to express the Green's function in terms of integrals that have to be evaluated numerically. In what follows, we will first present Ting's results for the anisotropic surface Green's function and then use it to derive the interaction energy of two force dipoles as well as an array of force monopoles corresponding to the Marchenko's periodic groove structure.

Using C_{ijkl} to denote the elastic constant tensor and employing polar coordinates (r, θ) defined so that $x = r\cos\theta$ and $z = r\sin\theta$, let us introduce the following 3×3 matrices,

$$\begin{aligned} \mathscr{Q}_{ik}(\theta) &= C_{ijks} n_j n_s, \\ \mathscr{R}_{ik}(\theta) &= C_{ijks} n_j m_s, \\ \mathscr{T}_{ik}(\theta) &= C_{ijks} m_j m_s, \end{aligned} \tag{A2}$$

where $\boldsymbol{n} = [\cos\theta, \sin\theta, 0]$ and $\boldsymbol{m} = [-\sin\theta, \cos\theta, 0]$. The anisotropic Green's function is expressed conveniently in terms of the following two matrices

$$\begin{aligned} \mathscr{N}_1(\theta) &= -\mathscr{T}(\theta)\mathscr{R}^{\mathrm{T}}(\theta), \\ \mathscr{N}_2(\theta) &= \mathscr{R}(\theta)\mathscr{T}^{-1}(\theta)\mathscr{R}^{\mathrm{T}}(\theta) - \mathscr{Q}(\theta), \end{aligned} \tag{A3}$$

and two incomplete integrals

$$\begin{aligned} \mathscr{S}(\theta) &= \frac{1}{\pi}\int_0^\theta \mathscr{N}_1(\omega)\,\mathrm{d}\omega, \\ \mathscr{L}(\theta) &= -\frac{1}{\pi}\int_0^\theta N_2(\omega)\,\mathrm{d}\omega. \end{aligned} \tag{A4}$$

Using these matrices, the anisotropic surface Green's function can be written as [35]

$$\mathscr{G}(r, \theta) = -\left[\frac{\log r}{\pi}\mathscr{I} + \mathscr{S}(\theta) - \frac{1}{2}\mathscr{S}\right]\mathscr{L}^{-1}, \tag{A5}$$

where $\mathscr{I}$ is the identity matrix, $\mathscr{S}=\mathscr{S}(\pi)$ and $\mathscr{L}=\mathscr{L}(\pi)$.

Let us now consider the interaction energy, $V^{\text{dipole}}(d)$, between two steps separated by a distance d with identical vector dipole force, $\mathbf{f}$. Let the steps that we label 1 and 2 be located at $(0, 0)$ and (d, a_z) respectively. Using the general formalism for interaction between two surface loads [18], we have

$$V^{\text{dipole}}(d)=-\int \mathscr{F}_2(x)\cdot\mathbf{u}_1(x, 0)\,\mathrm{d}x, \tag{A6}$$

where $\mathscr{F}_2(x)=\mathbf{f}\delta'(x-d)$ is the surface force density due to the step labeled 2 and $\mathbf{u}_1(x, z)$ is the displacement field produced by the step labeled 1. Noting that we can write

$$\mathbf{u}_1(x, z)=-\frac{\partial\,\mathscr{G}(x, z)}{\partial x}\mathbf{f}, \tag{A7}$$

and using the expression for the anisotropic surface Green's function in Eq. (A5) it can be shown that

$$V^{\text{dipole}}(d)=-\mathbf{f}\frac{\partial^2\mathscr{G}(d, 0)}{\partial^2 x}\mathbf{f}=\frac{\mathbf{f}\mathscr{L}^{-1}\mathbf{f}}{\pi d^2}. \tag{A8}$$

Using the above equation, we can now write a general expression for G (given in Eq. (10)) as

$$G=\frac{\mathbf{f}\mathscr{L}^{-1}\mathbf{f}}{\pi a_x^2}. \tag{A9}$$

In order to make the connection of our discrete model to Marchenko's groove structure, let us now consider the interaction energy $V^{\text{dipole}}(d)$ between two identical force monopoles, with surface force $\mathbf{F}$, located at $(0, 0)$ and $(d, 0)$. Following the same procedure that was used to derive the interaction energy between force dipoles, it is readily seen that

$$\begin{aligned}V^{\text{dipole}}(d)&=-\mathbf{F}\mathscr{G}(d, 0)\mathbf{F}\\&=\mathbf{F}\left[\frac{\log d}{\pi}\mathscr{I}-\frac{1}{2}\mathscr{S}\right]\mathscr{L}^{-1}\mathbf{F}.\end{aligned} \tag{A10}$$

If the two monopoles that we consider have the same magnitude, but opposite direction, then the interaction energy is the negative of the energy that we have derived in Eq. (A10). Using these results, it is straightforward to show that the energy of Marchenko's periodic groove structure in an anisotropic solid is identical to Eq. (18) with G given by

$$G=\frac{1}{\pi}\mathbf{F}\mathscr{L}^{-1}\mathbf{F}. \tag{A11}$$

Now, if our bunch phases and Marchenko's groove picture should be identical in energy, we require that G given by both Eq. (A9) and Eq. (A11) should be identical. It is easily seen that this indeed is true, since the relation $\mathbf{F}=\mathbf{f}/a_x$ that we proved in Eq. (23), holds for all types of crystalline solids.

Appendix B: Free energy of an inclined single step in the TSK model

In this appendix we derive the free energy of a single step placed on a rectangular lattice with lattice constants (a_x, a_y). The step runs on the average at an angle α with respect to the y-axis (The straight step has $\alpha=0$.). The slope of the step with respect to the y-axis is then $\hat{s}=\tan\alpha$. If the free energy per unit length of the step as a function of $\hat{s}$ is $\hat{f}(\hat{s})$, then in the expansion for small $\hat{s}$

$$\hat{f}(\hat{s})=\hat{f}_0+\frac{1}{2}\Sigma\hat{s}^2+\cdots, \tag{B1}$$

where Σ is the step stiffness. To compute $\hat{f}(\hat{s})$, it is easier to compute first the Legendre-transformed free energy

$$\hat{f}(\hat{\eta})=\hat{f}(\hat{s})-\hat{\eta}\hat{s}, \tag{B2}$$

where $\hat{\eta}$ is a field coupling to the slope $\hat{s}$ [18]. We assume that in going from one row to the next, the step can follow only three paths. It can go straight to the next row up with energy ϵ_0, to the left one column and then up one row with total energy $\epsilon_0+\Gamma-\hat{\eta}$, or to the right one column and then up one row with total energy $\epsilon_0+\Gamma+\hat{\eta}$. The partition function for the step is readily found, yielding the free energy

$$\begin{aligned}a_y\hat{f}(\hat{\eta})=\epsilon_0-k_{\mathrm{B}}T\ln\{&1+\exp[-\beta(\Gamma-\eta)]\\&+\exp[-\beta(\Gamma+\eta)]\}.\end{aligned} \tag{B3}$$

Combining Eqs. (B1)–(B3) yields (noting that

$e^{-\beta\Gamma} \ll 1$ for this model to apply), we obtain Eq. (13) of the text.

Appendix C: Quantum Monte Carlo Methods

C1. Variational Monte Carlo method

This is the simplest way of performing a quantum Monte Carlo simulation. Here, our aim is to have a trial wave function that has a set of parameters that can be varied. One then optimizes these parameters so as to obtain the lowest possible energy. By means of a Monte Carlo simulation, one can compute the energy of a wave-function as a function of the parameters. We start with writing the trial state $|\psi_T\rangle$ in terms of the configurations of the 1D lattice system

$$|\psi_T\rangle = \sum_R |R\rangle\langle R|\psi_T\rangle, \tag{C1}$$

where the coefficients $\langle R|\psi_T\rangle$ depend on the set of variational parameters p_i. Here, $|R\rangle$ is a state in configuration space. For example, for N bosons on L sites a configuration could be a state with bosons on lattice sites $[i_1, i_2, \ldots, i_N]$ such that $1 \le i_k \le L$ for $1 \le k \le N$. The expectation value of the energy in the state $|\psi_T\rangle$ can be expressed as

$$E_T = \frac{\langle\psi_T|\ \mathscr{H}|\psi_T\rangle}{\langle\psi_T|\psi_T\rangle} = \frac{\sum_R E_L(R)\langle\psi_T|R\rangle\langle R|\psi_T\rangle}{\sum_R \langle\psi_T|R\rangle\langle R|\psi_T\rangle}, \tag{C2}$$

where the local energy in configuration R is defined as

$$E_L(R) = \frac{\langle\psi_T|\ \mathscr{H}|R\rangle}{\langle\psi_T|R\rangle}. \tag{C3}$$

The sum in Eq. (C2), in general impossible to evaluate analytically, can be evaluated by Monte Carlo. One considers the following expression:

$$E_T = \sum_R E_L(R)p(R), \tag{C4}$$

where one interprets

$$p(R) = \frac{\langle\psi_T|R\rangle\langle R|\psi_T\rangle}{\sum_R \langle\psi_T|R\rangle\langle R|\psi_T\rangle} \tag{C5}$$

as a probability density function. If one then samples M configurations distributed according to $p(R)$ then the exact expression for E_T can be approximated by

$$E_{VMC} = \frac{\sum'_R E_L(R)}{M}, \tag{C6}$$

where the prime is used to represent the sum over the configurations. In the limit of large M, E_{VMC} will converge to E_T. The average E_{VMC}, of course, is subject to statistical fluctuations, and one can easily evaluate the statistical error by $\delta E = \sigma_E/\sqrt{M}$. The variance of the local energy, σ_E , is defined as

$$\sigma_E = \sqrt{\langle E^2\rangle - \langle E\rangle^2}, \tag{C7}$$

where $\langle E\rangle = E_{VMC}$ and $\langle E^2\rangle = \sum'_R E_L^2(R)/M$. It is known [36] that σ_E, which has a lower bound of 0, is a better quantity to optimize than E_{VMC}. We use both quantities as indicators in our search of variational parameters. For each set of variational parameters, we use the Metropolis algorithm to generate a set of M configurations distributed according to $p(R)$. We start with a configuration of M walkers each of which has N bosons randomly distributed on a lattice of 1D ring of size L. Each walker then undergoes a 'stochastic walk' according to the following procedure: (1) for each boson we pick a near neighbor site randomly and (2) if the site is occupied the boson is not moved, but if the site is empty the boson is moved with probability q given by

$$q = \min\left[1, \frac{\psi_T^2|_{new}}{\psi_T^2|_{old}}\right], \tag{C8}$$

where $\psi_T^2|_{new(old)}$ is $\langle\psi_T|R\rangle\langle R|\psi_T\rangle$ evaluated at R_{new} and R_{old}. This process is repeated a sufficient number of times so that one ends up with a set of walkers distributed according to $p(R)$.

C2. Green's function Monte Carlo method

This is in principle an exact way to calculate the ground state properties of Bose systems. Its required computer time scales algebraically (as opposed to exponentially in exact diagonalization) with system size, thus allowing exact calculations

for large systems. Here, one combines random sampling with a simple method to project out the ground state from an arbitrary initial state.

We start with the operator

$$\mathscr{F} \equiv C - \mathscr{H}, \tag{C9}$$

where the constant C, whose choice we discuss below, is to ensure that all matrix elements $\langle R'|\mathscr{F}|R\rangle$ are non-negative. The basic premise of GFMC is that repeated application of $\mathscr{F}$ on an essentially arbitrary initial state will project out the ground state. That is, if an initial state $|\psi^{(0)}\rangle$ has any overlap with the ground state $|\psi_0\rangle$ of $\mathscr{H}$, the process

$$|\psi^{(n)}\rangle = \mathscr{F}^n|\psi^{(0)}\rangle \tag{C10}$$

will lead to $|\psi_0\rangle$ at large n. GFMC is a method to realize the above process by a Monte Carlo random walk.

In order to improve efficiency of the random walk process, one more mathematical manipulation of Eq. (C10) is necessary. This is done by introducing an operator $\tilde{\mathscr{F}}$ whose matrix elements are related to those of $\mathscr{F}$ by a similarity transformation:

$$\mathscr{F}(R', R) \equiv \langle\psi_T|R'\rangle\langle R'|\mathscr{F}|R\rangle/\langle\psi_T|R\rangle. \tag{C11}$$

The stochastic realization of Eq. (C10) is actually with $\tilde{\mathscr{F}}$ instead of $\mathscr{F}$. While mathematically equivalent, the use of $\tilde{\mathscr{F}}$ can significantly reduce the fluctuation of the Monte Carlo process if $|\psi_T\rangle$ is a reasonable approximation of $|\psi_0\rangle$. This is known as importance sampling [26,27].

The program is then to start with a set of walkers distributed according to $\langle\psi_T|R\rangle\langle R|\psi_T\rangle$. These walkers undergo random walks in R-space. For each walker, denoted by R, taking a step in the random walk means randomly selecting and moving to a new position R' with probability $\tilde{\mathscr{F}}(R', R)/\sum_{R'}\tilde{\mathscr{F}}(R', R)$. Note that, because of the structure of $\mathscr{H}$, there are only $\mathcal{O}(N)$ possible R's and the corresponding probabilities can be easily computed. Because the overall normalization $\sum_{R'}\tilde{\mathscr{F}}(R', R)$ is not a constant, each walker carries an overall weight which fluctuates, or a branching scheme is introduced to allow the total number of walkers to fluctuate, or both.

The ground state energy is given exactly by the so-called *mixed estimate*

$$E_0 = \frac{\langle\psi_T|\,\mathscr{H}|\psi_0\rangle}{\langle\psi_T|\psi_0\rangle} = \frac{\sum_R E_L(R)\langle\psi_T|R\rangle\langle R|\psi_0\rangle}{\sum_R \langle\psi_T|R\rangle\langle R|\psi_0\rangle}, \tag{C12}$$

where $E_L(R)$ is defined in Eq. (C3). After a sufficient number of steps, the walkers are distributed according to $\langle\psi_T|R\rangle\langle R|\psi_0\rangle$. E_0 can therefore be computed from such walkers as the (weighted) average of $E_L(R)$ with respect to walker positions R, similar to Eq. (C6). We denote this Monte Carlo estimate of E_0 by E_{GFMC}.

Expectation values of operators other than $\mathscr{H}$ can also be computed from the mixed estimate. However, if the operator does not commute with $\mathscr{H}$, this estimate is *not* exact. As we mention in Section 5, this is an important distinction which requires careful analysis of the results. There exist ways to improve upon the mixed estimate and possibly to extract exact estimates of expectation values [26,37,38], but we will not discuss them here.

Now we describe our choice of C. Since we are dealing with a finite number of hard-core bosons on a lattice of finite size, the eigenstates of $\mathscr{H}$ are bounded both from above and below. If E_{max} is the highest eigenvalue of $\mathscr{H}$, we choose C such that $C > E_{max}$. This is easily achieved for the problem at hand. On the lattice we put all bosons next to one another and compute the potential energy arising from the long-range interactions alone. For N bosons, we choose C as

$$C = 2N + g\sum_{i=1}^{N-1}\frac{N-i}{i^2}. \tag{C13}$$

This clearly satisfies $C > E_{max}$, since hopping and the short-range attraction can only lower this energy.

References

[1] S. Song, S.G.J. Mochrie, Phys. Rev. Lett. 73 (1994) 995.
[2] S. Song, S.G.J. Mochrie, Phys. Rev. B 51 (1995) 10068.
[3] S. Song, M. Yoon, S.G.J. Mochrie, G.B. Stephenson, S.T. Milner, Surf. Sci. 372 (1997) 37.

[4] M. Yoon, S.G.J. Mochrie, M.W. Tate, S.M. Gruner, E.F. Eikenberry, Surf. Sci. 411 (1998) 70.
[5] K. Sudoh, T. Yoshinobu, H. Iwasaki, E.D. Williams, Phys. Rev. Lett. 80 (1998) 5152.
[6] K. Sudoh, T. Yoshinobu, H. Iwasaki, E.D. Williams, Scanning Microsc. 8 (1998) 9.
[7] M. Lässig, Phys. Rev. Lett. 77 (1996) 526.
[8] S.M. Bhattacharjee, Phys. Rev. Lett. 76 (1996) 4568.
[9] S.M. Bhattacharjee, S. Mukherji, Phys. Rev. Lett. 83 (1999) 2374.
[10] V.I. Marchenko, Sov. Phys. JETP 54 (1981) 605.
[11] C. Jayaprakash, C. Rottman, W.F. Saam, Phys. Rev. B 30 (1984) 6549.
[12] V.B. Shenoy, S. Zhang, W.F. Saam, Phys. Rev. Lett. 81 (1998) 3475.
[13] P.G. de Gennes, J. Chem. Phys. 48 (1968) 2257.
[14] M. den Nijs, in: C. Domb, J.L. Lebowitz (Eds.), Phase Transitions and Critical Phenomena Vol. 12, Academic Press, London, 1989.
[15] E. Le Goff, L. Barbier, L. Mason, B. Salanon, Surf. Sci. 432 (1999) 139.
[16] G.D. Mahan, Many-Particle Physics Sec. 1.4 A Plenum, New York, 1981.
[17] V.I. Marchenko, A.Ya. Parshin, Sov. Phys. JETP 52 (1981) 129.
[18] P. Nozières, in: C. Godrèche (Ed.), Solids Far From Equilibrium, Cambridge University Press, Cambridge, 1991.
[19] A.C. Redfield, A. Zangwill, Phys. Rev. B 46 (1992) 4289.
[20] J. Frohn, M. Giesen, M. Poensgen, J.F. Wolf, H. Ibach, Phys. Rev. Lett. 67 (1991) 3543.
[21] J.C. Heyraud, J.J. Métois, J. Cryst. Growth 50 (1980) 571.
[22] J.C. Heyraud, J.J. Métois, Acta Metall. 28 (1980) 1789.
[23] W.H. Press, S.A. Teukolsky, W.T. Vetterling, B.P. Flannery, Numerical Recipies in Fortran, Cambridge University Press, Cambridge, 1987.
[24] T.W. Burkhardt, P. Schlottmann, J. Phys. A 26 (1993) L501.
[25] B. Sutherland, J. Math. Phys. 12 (1971) 246.
[26] M.H. Kalos, Phys. Rev. 128 (1962) 1791.
[27] D.M. Ceperley, M.H. Kalos, in: K. Binder (Ed.), Monte Carlo Methods in Statistical Physics, Springer, Heidelberg, 1979.
[28] N. Trivedi, D.M. Ceperley, Phys. Rev. B 41 (1990) 4552.
[29] S. Zhang, N. Kawashima, J. Carlson, J.E. Gubernatis, Phys. Rev. Lett. 74 (1995) 1500.
[30] S. van Dijken, H.J.W. Zandvliet, B. Poelsema, Phys. Rev. B 55 (1997) 7864.
[31] J.-H. Zhu, K. Brunner, G. Abstreiter, Appl. Phys. Lett. 73 (1998) 2438.
[32] C. Duport, P. Nozières, J. Villain, Phys. Rev. Lett. 74 (1995) 134.
[33] D. Kandel, J.D. Weeks, Phys. Rev. Lett. 74 (1996) 3632.
[34] L.E. Shilkrot, D.J. Srolovitz, Phys. Rev. B 53 (1996) 11 120.
[35] T.C.T. Ting, Q.J. Mech, Appl. Math. 45 (1992) 119.
[36] C.J. Umrigar, K.G. Wilson, J.W. Wilkins, Phys. Rev. Lett. 60 (1988) 1719.
[37] K.J. Runge, Phys. Rev. B 45 (1992) 7229.
[38] S. Zhang, M.H. Kalos, J. Stat. Phys. 70 (1993) 515.